

Light-Activated siRNA Endosomal Release (LASER) by Porphyrin Lipid Nanoparticles

Yulin Mo, Miffy H. Y. Cheng, Andrew D'Elia, Katie Doran, Lili Ding, Juan Chen,* Pieter R. Cullis, and Gang Zheng*



Cite This: *ACS Nano* 2023, 17, 4688–4703



Read Online

ACCESS |

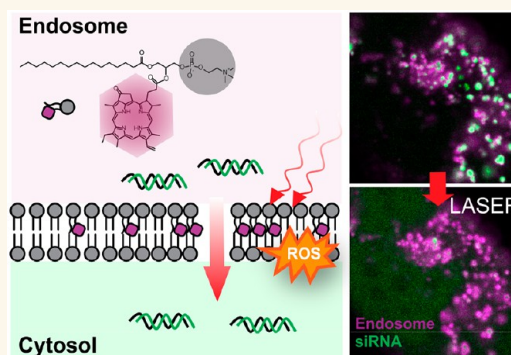
Metrics & More

Article Recommendations

Supporting Information

ABSTRACT: Lipid nanoparticles (LNPs) have achieved clinical success in delivering small interfering RNAs (siRNAs) for targeted gene therapy. However, endosomal escape of siRNA into the cytosol remains a fundamental challenge for LNPs. Herein, we report a strategy termed light-activated siRNA endosomal release (LASER) to address this challenge. We established a porphyrin-LNP by incorporating porphyrin-lipids into the clinically approved Onpattro formulation. The porphyrin-LNP maintained the physical properties of an LNP and generated reactive oxygen species (ROS) when irradiated with near-infrared (NIR) light. Using confocal microscopy, we revealed that porphyrin-lipids within the LNP translocate to endosomal membranes during endocytosis. The translocated porphyrin-lipids generated ROS under light irradiation and enabled LASER through endosomal membranes disruption as observed through GAL-9 recruitment and transmission electron microscopy (TEM). By establishing a quantitative confocal imaging method, we confirmed that porphyrin-LNPs can increase siRNA endosomal escape efficiency by up to 2-fold via LASER and further enhance luciferase target knockdown by 4-fold more in luciferase-transfected prostate cancer cells. Finally, we formulated porphyrin-LNPs encapsulated with gold nanoparticles (GNP) and visualized the LASER effect within prostate tumors via TEM, confirming the light-activated endosomal membrane disruption and subsequent GNP release into cytosols *in vivo*. Overall, porphyrin-LNPs and the LASER approach enhanced siRNA endosomal escape and significantly improved knockdown efficacy. We believe the versatility of this technology could be applied to various LNP-based RNA therapeutics.

KEYWORDS: lipid nanoparticles, porphyrin lipid, nanomedicine, RNA delivery, endosomal escape, photochemical internalization, photosensitizer



INTRODUCTION

RNA interference (RNAi) is an exciting addition to the therapeutic toolkit for targeted gene therapies. Small interfering RNAs (siRNAs) are the key molecules that enter the RNAi pathway after cytosolic delivery. They are loaded into the RNA-induced silencing complex (RISC) and selectively silence the expression of complementary genes.^{1–3} Diverse delivery systems have been developed to deliver intact siRNA to *in vivo* targets, such as viral and nonviral vectors. Among these systems, lipid nanoparticles (LNPs) served as the first carrier platforms that have led to the FDA-approval of an siRNA drug against transthyretin-induced amyloidosis, namely, Onpattro in 2018.^{4–6} Despite the clinical success of LNP-siRNA, the extremely low siRNA endosomal escape efficiency (1–2%) after LNP endocytosis is a major hindrance in LNP-based siRNA delivery.⁷ Consequently, the majority of siRNAs are either degraded in the lysosomes or exocytosed from the cells,⁸ severely impairing their therapeutic efficacy. Thus, a more

efficient LNP system that can improve siRNA cytosolic delivery is crucially needed.

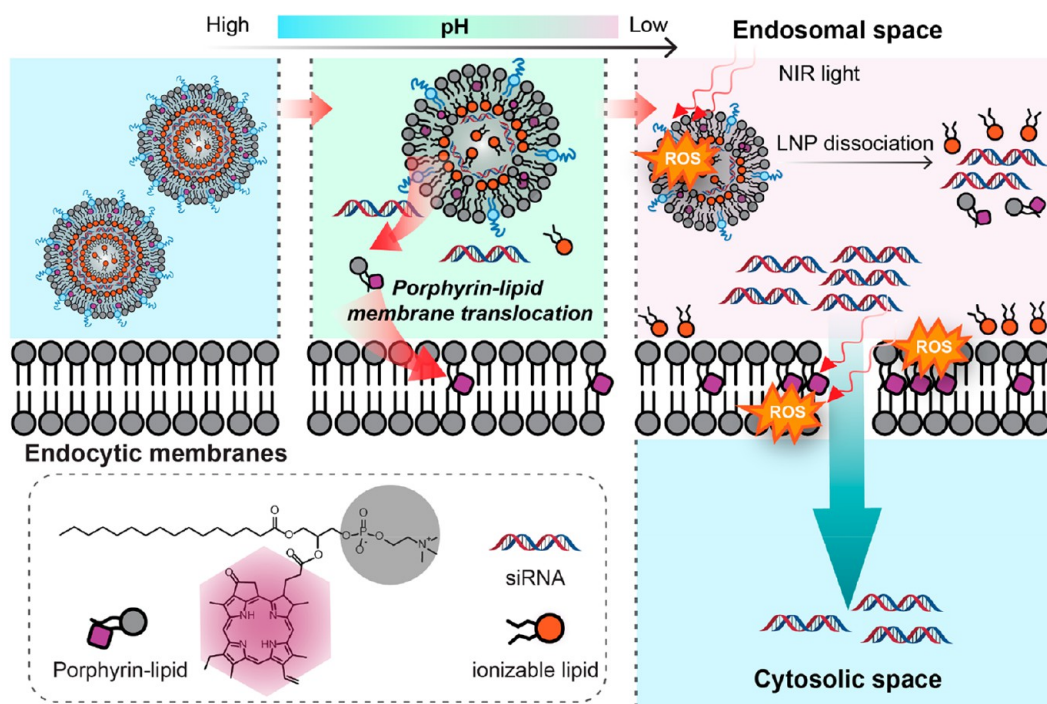
One method is to introduce a stimulus-sensitive component into LNPs that responds to a specific external trigger and subsequently releases the cargo into cytosol. Previously, researchers have utilized light as a noninvasive, adjustable stimulus to facilitate endosomal escape of macromolecules. Light can induce local photothermal effect via plasmonic gold nanoparticles to create transient pores on endolysosomal structures, which allows various macromolecules to escape from the endosomes and associated vesicles.^{9–11} In addition,

Received: November 2, 2022

Accepted: February 22, 2023

Published: February 28, 2023



Scheme 1. Schematic Illustration of Porphyrin-LNP Mediated LASER Approach^a

^aAfter porphyrin-LNP endocytosis, LNPs become less intact as pH decreases in acidic organelles. Dissociated porphyrin-lipids then partially and progressively translocate to endocytic organelle membranes due to their lipophilicity. Once cells are irradiated with NIR light, ROS generated by porphyrin-lipids enhances both LNP dissociation and damages endocytic membranes, which ultimately leads to improved siRNA endosomal escape into the cytosolic space.

light can also induce chemical reactions on endosomal membrane to allow cargo escape in an approach termed photochemical internalization (PCI).^{12–14} Typically, PCI requires a photosensitizer (PS) to be embedded within cell endosomal membranes, which can generate reactive oxygen species (ROS) upon exposure to light in a controlled manner. The resulting ROS would subsequently destabilize endosomal membranes and release trapped macromolecules into the cytosol. Although the PCI approach has demonstrated improved cytosolic delivery of various macromolecules *in vitro* and good tolerability in human patients,^{14–16} traditional PCI is limited by the need for a two-step delivery process, wherein PS must be administered prior to the therapeutic agents. The resulting inconsistent distribution of PS and macromolecules to target cells largely hinders its applications *in vivo*. To alleviate the two-step requirement, a few exploratory studies have applied PS-siRNA conjugates,^{17–19} polymeric and liposome-based siRNA carriers to improve siRNA endosomal escape via PCI.^{20–22} Nevertheless, such systems are still limited by (1) the synthetic and scalable challenges to chemically link PS and siRNA;²³ (2) the premature leakage of small-molecule PS from siRNA nanocarriers;²⁴ (3) the poor biocompatibilities of cationic siRNA carriers;²⁵ and last (4) the lack of direct evidence supporting proposed PCI mechanisms (*e.g.*, PS localization on endocytic membranes, changes in membrane integrity). Given the great clinical successes already achieved by LNPs in delivering siRNA and mRNA, PCI systems built upon LNPs will be highly translatable by addressing the unmet RNA endosomal escape challenge. Therefore, implementing a PS that is simple, compatible with LNP systems, and fully understand its light-activated release mechanisms in the context of LNPs

becomes the ultimate key in designing next-generation light-activatable LNPs.

Porphyrin-lipid is a phospholipid-porphyrin conjugate discovered by our group in 2011. It is both a photosensitizer and a nanoparticle building block that can be stably incorporated within diverse lipid-based nanoparticles (liposomes, HDL-like nanoparticles, microbubbles, and nanoemulsions).^{26–29} Nanoparticles composed of porphyrin-lipid building blocks can produce ROS when irradiated with near-infrared (NIR) light, and are widely used for photodynamic therapy (PDT),^{30–32} a clinically used treatment modality that forms the basis for PCI. Considering the ease of porphyrin-lipid to self-assemble into lipid-based nanoparticles, and its intrinsic nature as a photosensitizer to generate ROS, porphyrin-lipids are a promising candidate that can be incorporated into the clinically used LNP formulations to improve siRNA endosomal escape following a similar strategy to PCI.

Herein we report the development of porphyrin-lipid nanoparticles (porphyrin-LNPs) and demonstrate the Light-Activated SiRNA Endosomal Release (LASER) approach. Porphyrin-LNPs were engineered by replacing helper lipids from the clinically approved Onpatro formulation with porphyrin-lipids, which maintained its colloidal properties while conferring the photoactive properties of porphyrin to the LNP. Using systemic imaging experiments, we found that porphyrin-LNPs can enable LASER across various cancer cell lines originated from different tissue types (PC3, 4T1, PANC-1, A549, SKOV-3). Mechanistic imaging studies have confirmed that porphyrin-LNPs triggers LASER via the gradual translocation of the porphyrin-lipid from the LNPs to the endosomal membrane and subsequent membrane-specific ROS damage (Scheme 1). Since many previous studies on RNA endosomal

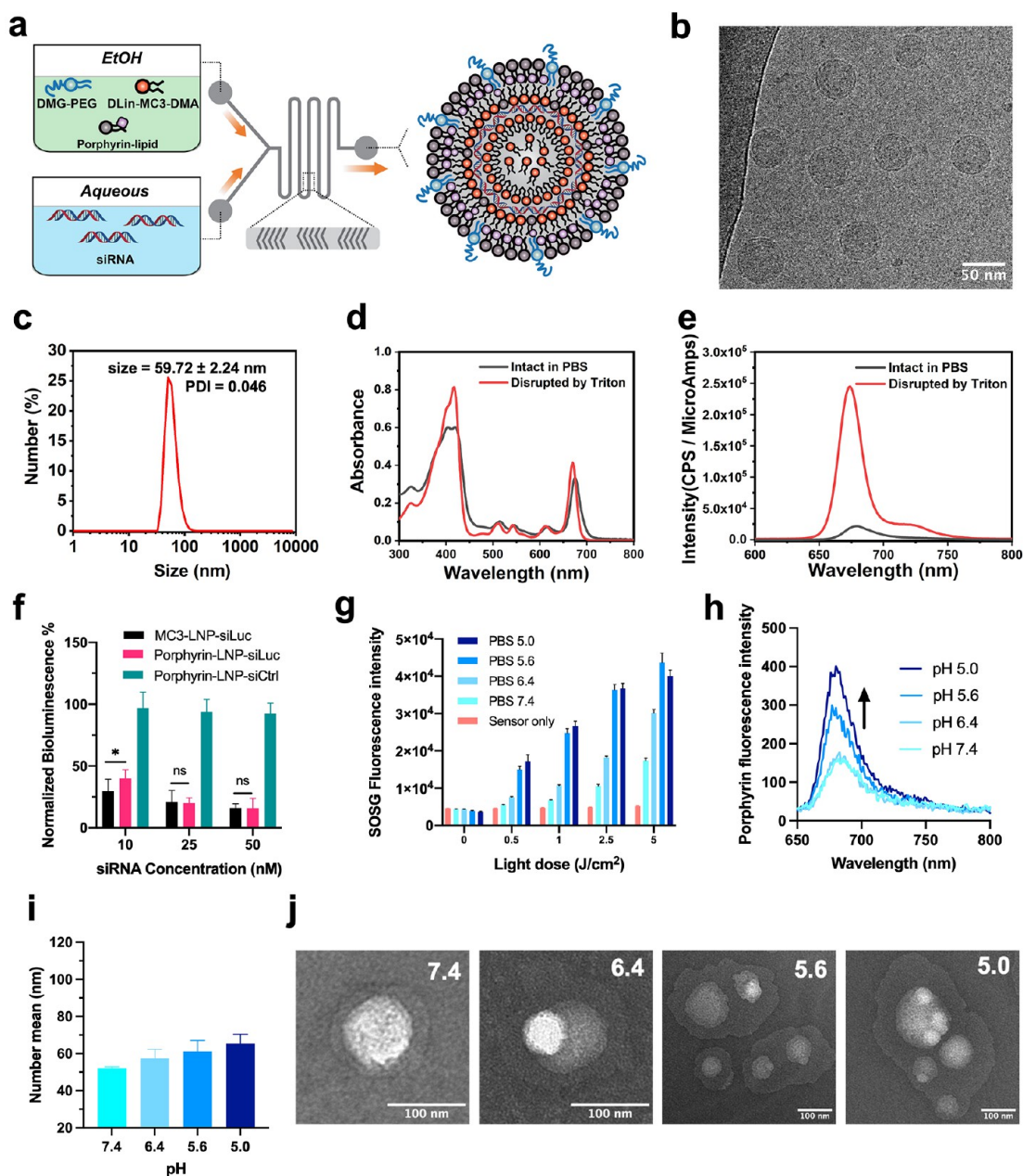


Figure 1. Synthesis and characterization of porphyrin-LNP. (a) Porphyrin-LNPs were synthesized via rapid mixing through a herringbone microfluidic chip. (b) Cryo-TEM image of porphyrin-LNP. (c) Size distribution of porphyrin-LNP measured by DLS. (d) Representative absorption and (e) fluorescence spectra (Ex: 410 nm) of intact and disrupted porphyrin-LNPs. (f) Luciferase expression of PC3-Luc6 cells treated with various LNPs at 10, 25, and 50 nM siRNA concentration for 24 h. Bioluminescence was normalized to untreated control cells. * $p < 0.05$. Data are presented as means \pm standard deviation ($n = 3$). (g) Singlet oxygen generation from porphyrin-LNPs upon 671 nm irradiation. (h) Emission spectrum of porphyrin-LNPs when dispersed in PBS at different pH (Ex: 410 nm). (i) Size distribution of porphyrin-LNP after dilution to PBS with corresponding pH solution. (j) TEM images of porphyrin-LNP at varying pH condition.

escape relied on qualitative data to evaluate release (e.g., RNA colocalization with endocytic vesicle markers), there is a lack of quantitative measurements of siRNA endosomal escape efficiency. Therefore, we also established a quantitative analyzing pipeline based on 3D confocal imaging data and unveiled that the siRNA endosomal escape efficiency delivered by porphyrin-LNPs can be doubled when light was applied. The quantitative data from imaging studies is also consistent with *in vitro* knockdown results where porphyrin-LNPs significantly decreased the required siRNA dose (~ 4 -fold) to achieve target mRNA silencing using LASER strategy. Lastly, we provided

early evidence for light-induced organelle membrane disruption by porphyrin-LNPs *in vivo* using TEM imaging. Overall, we have demonstrated a significant improvement of siRNA endosomal escape through porphyrin-LNP-mediated LASER approach and provided mechanistic insights of its distinctive function that enabled higher cytosolic release rate of the siRNA entrapped with the LNPs.

RESULTS AND DISCUSSION

Porphyrin-LNP Synthesis and Characterization. Porphyrin-LNPs were synthesized using a standard rapid mixing

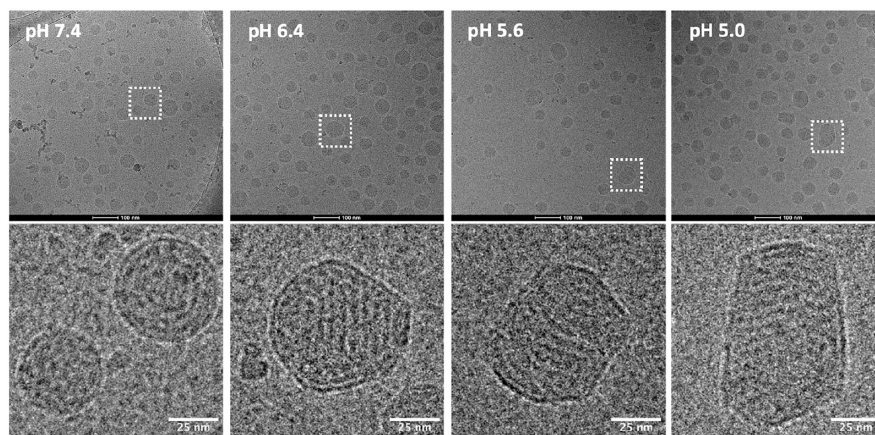


Figure 2. Cryo-TEM images of porphyrin-LNP at different pH conditions.

method through a microfluidic system (Figure 1a).³³ We first prepared porphyrin-LNP by modifying the Onpattro formulation and replacing all the helper lipid DSPC with porphyrin-lipid, at a molar ratio of 50/10/38.5/1.5 (MC3-lipid/Porphyrin-lipid/Cholesterol/DMG-PEG₂₀₀₀). Porphyrin-LNP formulations had >95% siRNA encapsulation efficiency and $81.3 \pm 6.0\%$ siRNA recovery rate as determined by Ribogreen assay. They displayed spherical amorphous core structures under cryo-TEM, with homogeneous size distribution at 59.72 ± 2.24 nm (polydispersity index (PDI) < 0.1) as measured by dynamic light scattering (Figure 1b,c). The siRNA encapsulation, morphology, and size of porphyrin-LNPs are comparable to those of LNP formulations with similar compositions,³³ suggesting the replacement of porphyrin-lipid at the expense of helper lipids did not compromise the LNP's colloidal properties. Given the intrinsic nature of porphyrin-lipid as a photosensitizer, we investigated the optical properties of the porphyrin-LNPs. The absorption of porphyrin-LNPs in both intact and disrupted states showed distinct porphyrin-based absorbance at 410 nm (Soret band) and at ~ 670 nm (Q-band) (Figure 1d). Compared to disrupted porphyrin-LNPs, the porphyrin fluorescence was highly quenched for the intact porphyrin-LNPs at 676 nm (quenching efficiency $\sim 91.2\%$). This was due to porphyrin-lipid self-quenching within the LNP nanostructure (Figure 1e).²⁶ To evaluate whether the replacement of the helper lipid with porphyrin-lipid would influence transfection potency, we performed *in vitro* siRNA knockdown experiments using a prostate cancer cell line expressing luciferase (PC3-Luc6). As shown in Figure 1f, the porphyrin-LNP-siLuc and the positive control of MC3-LNP-siLuc (Onpattro formulation) both effectively silenced 60%–80% luciferase expression at siRNA concentrations from 10 to 50 nM, while all negative controls of siCtrl-loaded LNPs showed no luciferase knockdown. Although a slight decrease in siRNA transfection potency was observed at 10 nM siRNA dose in porphyrin-LNP (60% knockdown) compared to Onpattro (70%), in general replacing 10 mol % DSPC helper lipids with porphyrin-lipid has minimal impact to the LNP's transfection potency. We then formulated porphyrin-LNPs with different porphyrin-lipid densities (2–20 mol %) and evaluated their silencing efficacy (Figure S1). Notably, except for 20 mol % porphyrin-lipid LNP that showed significantly poorer transfection efficacy across all concentrations, porphyrin-LNPs containing 2–10 mol % porphyrin-lipids demonstrated effective luciferase knockdown with negligible differences between each group. Therefore, the porphyrin-LNP containing

10 mol % porphyrin-lipid was carried forward to the following experiments.

We next investigated the generation of reactive oxygen species (ROS) from porphyrin-LNP upon light irradiation. As shown in Figure 1g, porphyrin-LNPs were capable of generating ROS under varying pH conditions that mimic environmental pH such as in early endosomes (~ 6.4), late endosomes (~ 5.6), and lysosomes (~ 5.0).^{34,35} Significant singlet oxygen sensor green (SOSG) fluorescence signal was observed in lower pH conditions (pH 5.6 and 5.0), suggesting that porphyrin-LNPs produced more ROS when exposing to more acidic environment. In comparison, completely disrupted porphyrin-LNPs showed overall comparable ROS generation across all tested pHs (Figure S2), which indicates that monomeric porphyrin-lipid ROS generation is not pH dependent. Similarly, intact porphyrin-LNP exhibited stronger porphyrin fluorescence at lower pH conditions whereas monomeric porphyrin-lipid has minimal changes in fluorescence intensity across different pH (Figures 1h and S3). The pH-dependent ROS production and fluorescence recovery of intact porphyrin-LNPs likely correspond to the LNP's gradual fusion and rearrangement events in an acidic environment, where ionizable lipids in LNPs become progressively protonated and interact with endogenous anionic membranes.³⁶ As a result of porphyrin-LNP fusion and lipid rearrangements, more porphyrin-lipids become unquenched at lower pH conditions, thereby generating more ROS upon irradiation. We further performed size and TEM imaging studies to confirm the pH effect on porphyrin-LNP. Porphyrin-LNP showed a slight increase in hydrodynamic size from 52 to 65 nm when pH decreased from 7.4 to 5.0 (Figure 1i). A further increase in size was noticed from 51 nm at pH 7.4 to 97 nm at pH 5.0 when LNPs were incubated at 37 °C for 24 h (Figure S4). TEM images also support larger LNPs forming at lower pH as a result of LNP fusion (Figures 1j and S5). Interestingly, small protrusions were observed to form on the LNP surface at pH 6.4, which might be an initial sign for subsequent LNP fusion, as for lower pH of 5.6 and 5.0, less protrusions were observed in those single LNPs while more protrusions were observed in the fused LNPs. Beyond TEM, cryo-TEM images (Figure 2) further revealed that LNPs have larger size at lower pH and changed their morphology from spherical (pH 7.4) to irregular multifaceted structures (pH 5.0), which also indicates fusion events and lipid rearrangement occurring within the LNPs when environmental pH decreases.

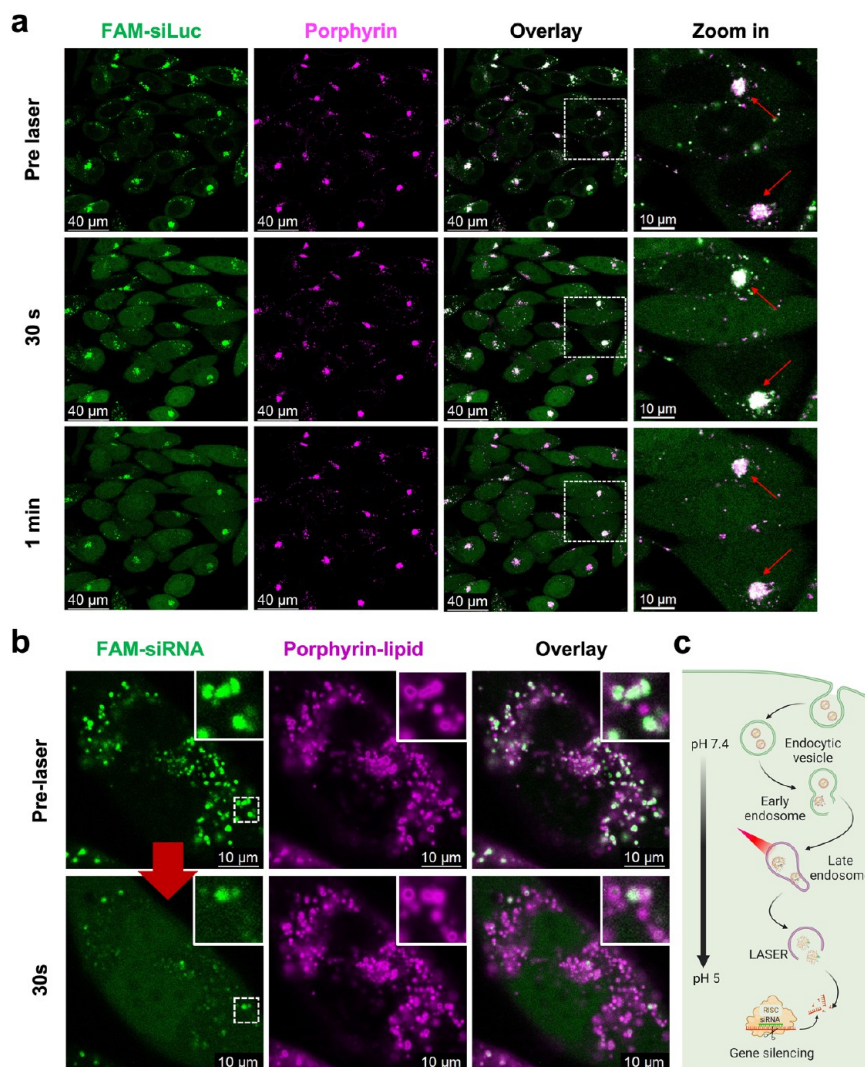


Figure 3. Visualization of LASER and porphyrin-lipid membrane translocation. (a) Confocal microscopy images of PC3-Luc6 after treatment with porphyrin-LNPs (FAM-siRNA) for 6 h. Significantly enhanced FAM-siRNA signal was observed in the cytosols post light irradiation at 660 nm. (b) Confocal microscopy images of PC3-Luc6 cells after incubating with porphyrin-LNPs for 24 h, before and post irradiation at 660 nm for 30 s. Porphyrin-lipids displayed vesicular structures, suggesting their translocation to endocytic organelle membranes. (c) Possible porphyrin-LNP endocytosis and porphyrin-lipid membrane translocation process.

One possible explanation for increased LNP size at lower pH is because more ionizable lipids in LNPs become positively charged at lower acidic pH, resulting in extra electrostatic repulsive force between these charged ionizable lipids. As a result, LNPs fuse to larger sizes to maintain the original positive charge density which is matched with the negative charges from the siRNA payload. Importantly, increased LNP size gives overall decreased nanoparticle surface area (surface area to volume ratio decreases at larger size), therefore fewer helper lipids are required to incorporate on the LNP surface. The extra surface helper lipids (porphyrin-lipid in our system) could possibly dissociate from LNPs, which correlates to the previous observations of porphyrin fluorescence recovery at lower pH. Additionally, at lower pH, LNPs are in a less intact “loosely assembled” status, which is indicated by more siRNA leakage when pH drops from 7.4 to 5.0 (Figure S6). Overall, at lower pH, fusion and lipid rearrangements of porphyrin-LNP lead to less intact LNP with larger size and stronger activation of porphyrin-lipid optical properties. Next, we studied the effect of

ROS generation on porphyrin-LNP morphology through DLS and TEM (Figure S7). A slight decrease in LNP size was noticed in the presence of $1.5\text{ J}/\text{cm}^2$ irradiation, along with less visible protrusions on LNP surface and less LNP clusters at lower pH. This data indicates porphyrin-LNPs might induce LNP dissociation through interacting with ROS from light irradiation. As ROS generation from the porphyrin-LNP complement with the decreased LNP stability in acidic environment, light activation of the porphyrin-LNPs and generation of ROS can induce a more thorough endosomal membrane phase change beyond ionizable lipid-endosomal membrane fusion, which ultimately leads to more siRNA endosomal escape.

Next, we studied the *in vitro* stability of porphyrin-LNP (Figure S8). Porphyrin-LNPs were highly stable when stored at $4\text{ }^\circ\text{C}$ in PBS 7.4, with no significant change in size and siRNA encapsulation efficiency after 1 month (Figure S8a,b). In addition, porphyrin-LNPs were colloidal stable within 24 h under both buffer and serum conditions at $37\text{ }^\circ\text{C}$, determined by its fluorescence quenching efficiency (QE) as a metric of LNP

intactness. As shown in Figure S8c,d, the porphyrin-LNPs exhibited >90% QE and negligible QE changes in PBS over 24 h incubation. Similarly, porphyrin-LNPs still maintained >80% QE after 24 h incubation in 50% fetal bovine serum solution (representative of physiological serum concentration). The high QE of porphyrin-LNP in extracellular biological environment is a favorable property, as it minimizes ROS generation of intact LNP, which enables a more specific ROS production in the endocytic organelles when LNPs are dissociated and activated. We also measured siRNA release from porphyrin-LNPs at 37 °C for 24 h in cell culture medium EMEM + 10%FBS (Figure S8e). Surprisingly, ~50% siRNA was released out of LNPs after 3 h incubation and reached to a stable state after 6 h, with ~60% siRNA released and maintained until 24 h. This result indicates the need of improving LNP stability for future *in vivo* applications.

Porphyrin-LNPs Enabled Light-Activated siRNA Endosomal Release (LASER). To investigate porphyrin-LNP mediated LASER methodology, we visualized the subcellular localization of dye (FAM) labeled siRNA and porphyrin-lipid using confocal microscopy. First, porphyrin-LNP's subcellular colocalization in acidic organelles was confirmed via tracking porphyrin-LNP over time (at 1, 3, 6 h incubation) with costaining of early endosome, late endosome, and lysosome in cells (Figures S9–S12). Next, the effect of light irradiation on siRNA endosomal escape was studied (Figure 3a): we treated PC3-Luc6 cells with porphyrin-LNP encapsulated with FAM-labeled siRNA. After 6 h incubation, both green and magenta fluorescence signals (corresponding to FAM-siRNA and porphyrin-lipids) resided and colocalized in the punctate patterns (Pearson's $R = 0.70$), suggesting LNP and siRNA were both entrapped inside endolysosomal structures after endocytosis. Markedly, after 30 s *in situ* laser irradiation at 660 nm, a strong, well-distributed FAM-siRNA signal was observed in the cell cytosol, while the porphyrin signal maintained a punctate pattern, leading to a decreased Pearson's R (0.55) of the two signals. After another 30 s irradiation, the FAM-siRNA signal in the cytosol was enhanced further in some cells, while the porphyrin signal intensity and location remained unchanged. This observation suggests successful siRNA endosomal escape by porphyrin-LNP-enabled light activation. Interestingly, along with an increased FAM-siRNA signal in the cytosol post irradiation, the FAM-siRNA signal in some organelles revealed an "activation first—then release" pattern (indicated by red arrows in magnified view) where puncta color changed from slightly magenta to very white (1st irradiation) and then returned to slightly magenta (2nd irradiation), indicating the activation of FAM-siRNA in the endocytic organelles before their subsequent endosomal release. Therefore, we stipulated two potential mechanisms for porphyrin-LNP-enabled LASER: (1) light irradiation induced siRNA endosomal escape by destabilizing organelle membranes; (2) light irradiation facilitated siRNA dissociation from LNPs in the organelles where the LNP dissociation is not sufficient. Regardless of which mechanism, porphyrin-lipid played a critical role in LASER, as for LNPs without porphyrin-lipid (Figure S13a), the FAM-siRNA signal was mainly trapped in the endosomal organelles and showed no obvious increase in the cytosol following light irradiation. Furthermore, to ensure the increased green fluorescence in cytosol of Figure 3a was not a false-positive background signal attributed to side-products of ROS oxidation, we showed that porphyrin-LNPs loaded with nonfluorescent siRNA (Figure S13b) displayed a negligible green fluorescence

signal in the cytosol upon light irradiation. Next, we investigated whether the LASER strategy using porphyrin-LNP could be widely applicable among cells from different tissue types. As shown in Figure S14, before light irradiation, a similar punctate pattern of porphyrin-lipid and FAM-siRNA fluorescence in organelles was observed among breast cancer (4T1), pancreatic cancer (PANC-1), lung cancer (A549), and ovarian cancer (SKOV-3) cells. Similarly, a significant enhancement of cytosolic siRNA signal was observed across all cancer cell lines upon light irradiation, confirming porphyrin-LNP based LASER could be functional in a variety of cell and tissue types, and highlighting its potential to improve siRNA endosomal release in a range of diseases.

Although in previous experiments we attribute the marked siRNA cytosolic delivery to ROS-induced endosomal membrane disruption, the suborganelle localization of porphyrin-lipid (e.g., on membrane vs in lumen) is still unclear. As ROS only has a limited diffusion distance of 10–20 nm and very short lifetime ($<0.1 \mu\text{s}$),³⁷ the localization of PS within organelles can largely impact its photoactivity and functional mechanism. Thus, we applied high resolution confocal imaging to reveal the suborganelle localization of porphyrin-lipid to provide a more comprehensive understanding of porphyrin-LNP-enabled LASER. As shown in Figure 3b, after 24 h incubation of PC3-Luc6 cells with FAM-siRNA encapsulated porphyrin-LNP, the FAM-siRNA signal predominantly resided within the lumen of the punctate organelles, while the porphyrin-lipid signal displayed distinctive vesicular structures which surrounded the FAM-siRNA signals from the lumen. At 30 s post laser treatment, most punctate FAM-siRNA signals diminished from the lumen, and a migration of the FAM-siRNA signal can be clearly observed in the cytosol. No change in the location of porphyrin-lipid was observed as it remains in the vesicular structures. This real-time imaging evidenced the translocation of porphyrin-lipids from the LNPs to endocytic organelle membranes. We also observed that translocation of porphyrin-lipid to organelle membranes is a sequential event (Figure S15), as the porphyrin-lipid signal was predominantly observed in the lumen of the punctate organelles at earlier time points (6 h), but progressively concentrated onto organelle membranes at later time points (9 and 24 h), forming mostly vesicular structures. This indicates that, at early time points, the majority of the porphyrin-lipids were associated with the LNPs and remained in the endocytic organelles. As the LNP dissociates over time, porphyrin-lipids begin to translocate to organelle membranes due to its lipophilicity. Moreover, we observed, that at a longer incubation time (24 h), the diameter of organelles became larger. This observation supports the homotypic membrane fusion of endocytic organelles during their maturation process and the osmotic swelling of organelles as ionizable lipids became protonated in more acidic environments. Even though at earlier time points the majority of the porphyrin-lipid resided in the lumen, a small fraction of porphyrin-lipids on endocytic membranes would still be sufficient to induce efficient ROS generation and subsequent membrane disruption to facilitate cytosolic delivery of siRNA.

Altogether, the observations of porphyrin-lipid suborganelle location suggest that as porphyrin-LNPs are endocytosed and progressively dissociated in more acidic organelles, porphyrin-lipids can gradually and partially translocate to endocytic organelle membranes. Therefore, when irradiated by NIR light, membrane-specific ROS generation can be induced to release trapped siRNA into the cytosol as illustrated in Figure 3c.

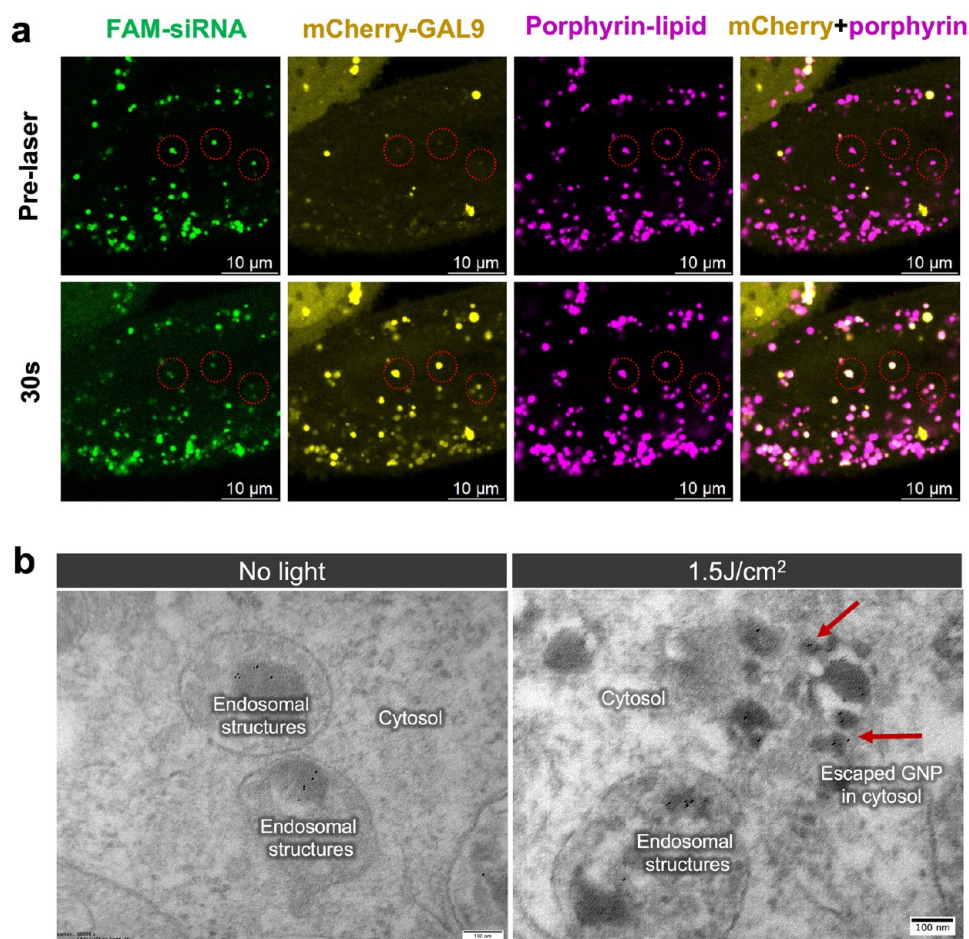


Figure 4. Endocytic membrane disruptions by porphyrin-LNP in LASER. (a) PC3-Luc6 cells expressing mCherry-galactin-9 (GAL9) were incubated with porphyrin-LNPs for 6 h and imaged by confocal microscopy before and post irradiation at 660 nm. Red dashed circles highlighted the organelles where both siRNA endosomal escape and galactin recruitment have occurred. (b) Representative TEM images of PC3-Luc6 cells after porphyrin-LNP-GNP treatment, with and without further light irradiation. Red arrows: escaped GNPs in cytosol.

Integrity Changes of Endocytic Organelle Membranes in LASER. To further investigate the mechanisms of porphyrin-LNP enabled LASER, we examined the integrity changes of endocytic organelle membrane under the LASER process as more direct evidence of membrane damage beyond siRNA endosomal release.

The integrity of endocytic organelle membranes upon light irradiation was first evaluated through imaging galactin-9 (GAL9) protein recruitment at sites of endosomal disruption.³⁸ PC3-Luc6 cells were transiently transfected with mCherry-GAL9 plasmids (Figure 4a), where mCherry-GAL9 proteins were mainly distributed in the cytosol with a weak, diffuse pattern. While few random organelles displayed punctate mCherry signal, the signal did not colocalize with siRNA or porphyrin. Immediately after 30s light irradiation, endocytic organelles displayed bright punctate mCherry signals, indicating GAL9 recruitment into the membrane-disrupted organelles. The bright mCherry signal also colocalized well with porphyrin-lipid signal (Pearson's R increased from 0.23 to 0.61 after irradiation), suggesting the correlation between ROS generation and endocytic membrane damage, as mCherry-GAL9 was mostly recruited to the sites where porphyrin-lipids were enriched. Moreover, in the organelles where noticeable siRNA release occurred (shown in red circles), pronounced mCherry-

GAL9 recruitment could be seen, further demonstrating the critical role of membrane disruption in LASER.

To further visualize organelle membrane integrity changes under LASER through TEM, gold nanoparticle (GNP)-loaded porphyrin-LNPs were synthesized by encapsulating 5 nm tannic acid coated GNPs into porphyrin-LNPs, as a substitute for siRNA (~7.5 nm in length and 2 nm in diameter).³⁹ A GNP recovery assay was performed by measuring the absorption of the GNP before and after the formulation process and a $92 \pm 5\%$ recovery of GNP in the porphyrin-LNP-GNP was confirmed. Moreover, we found that the % recovery remained >90% even after running through a Sephadex G-25 size exclusion column chromatography to remove any unloaded free GNPs. Synthesized porphyrin-LNP-GNPs were similar in size to siRNA-loaded porphyrin-LNPs and GNPs were successfully loaded in the core of LNPs as shown in cryo-TEM (Figure S16). PC3-Luc6 cells were incubated with porphyrin-LNP-GNP for 24 h and then treated either with or without 1.5 J/cm² light irradiation at 671 nm prior to subsequent imaging by TEM. As shown in Figure 4b, in the absence of light, GNPs were enclosed within the endosomal structures with clear membrane integrity. This observation was consistent with previous fluorescence microscopy images where the majority of the LNP-siRNA was trapped in endosomal structures after cellular uptake (Figure 4a). In comparison, with light irradiation at 1.5 J/

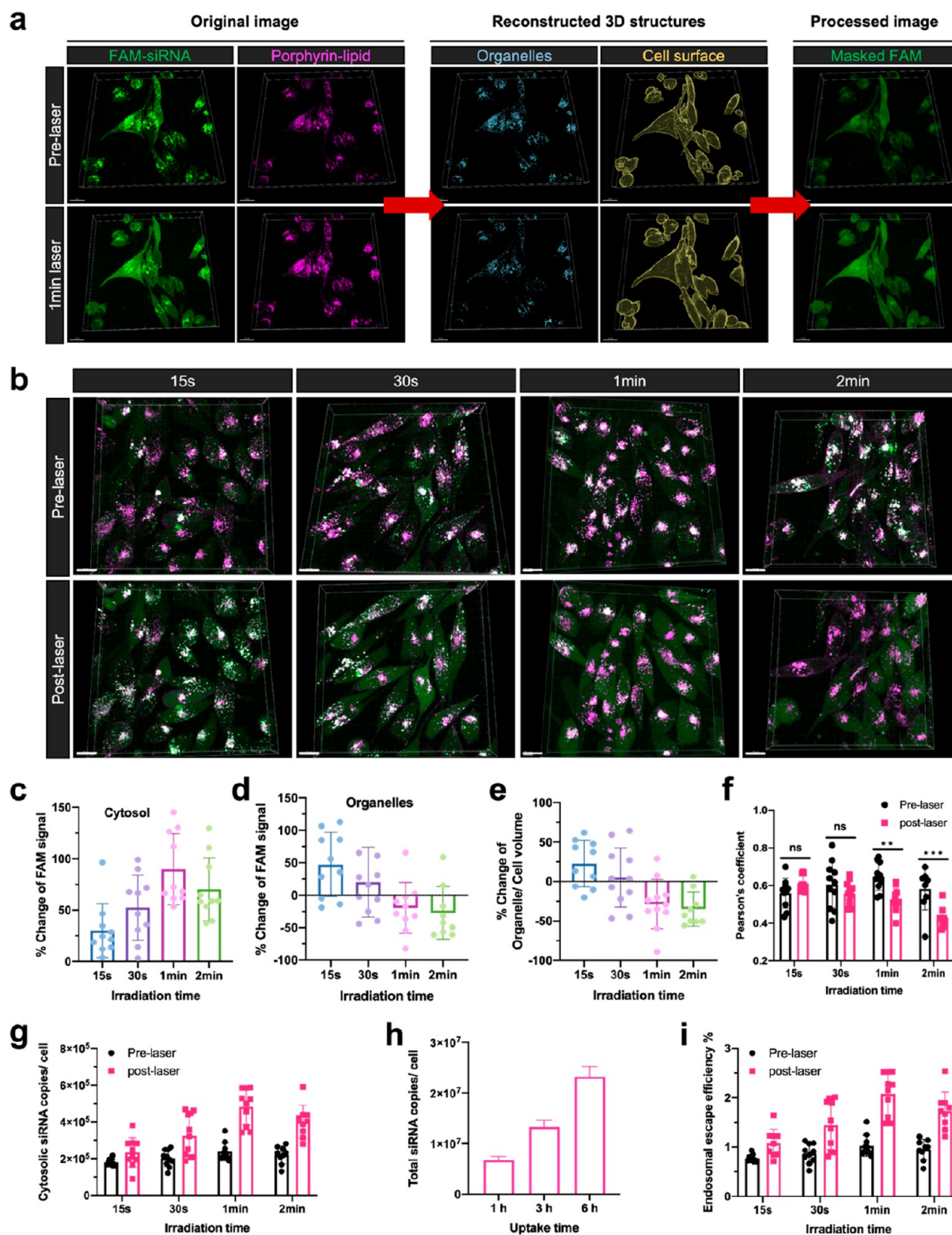


Figure 5. Quantitative analysis of siRNA endosomal release efficiency by porphyrin-LNPs. (a) Example of generating 3D quantitative data set: fluorescence from porphyrin-lipid and FAM-siRNA were captured across $20\ \mu\text{m}$ Z-stacks and reconstructed into 3D objects to identify organelles and cellular structures. Then FAM-siRNA signals from organelles were subtracted from original images to generate “masked FAM” images which only contain FAM-siRNA signal from the cytosolic space. Increased FAM-siRNA signal in cytosols was observed after light irradiation. Scale bar: $30\ \mu\text{m}$. (b) 3D confocal images of PC3-Luc6 cells after incubating with porphyrin-LNPs for 6 h, pre- and post-irradiation for varying time at 660 nm. Scale bar: $20\ \mu\text{m}$. (c,d) Quantitative analysis of FAM intensity sum % change pre- and post-irradiation in cytosol and organelles. (e) Percent change of organelle to cell volume pre- and post-irradiation. (f) Pearson’s colocalization coefficient between FAM-siRNA and porphyrin-lipid signal pre- and post-irradiation. ** $p < 0.01$, *** $p < 0.005$. For (c)–(g), each data point was generated from a whole 3D data set as illustrated in (a), which typically contains 10–20 individual cells. (g) Cytosolic FAM-siRNA copies per cell. (h) Total FAM-siRNA copies per cell. (i) Endosomal escape efficiency per cell.

Figure 5. continued

siRNA copies per cell at different cell uptake time. Porphyrin-LNPs were incubated with PC3-Luc6 cells at a concentration of 4 μ M porphyrin dose. Data are presented as means \pm standard deviation ($n = 3$). (i) siRNA endosomal escape efficiency pre- and post-irradiation after 6 h porphyrin-LNP incubation with cells, calculated from data in (g) and (h).

cm^2 , signs of endosomal membrane damage were observed, and some GNPs were found randomly distributed in the cytosol without the enclosure of any membrane structures. This confirmed that light triggered the escape of GNPs into cytosols as the result of the endocytic organelle membrane damage. To eliminate the possibility of membrane disruption caused by any photothermal effect generated from GNPs upon light irradiation, we synthesized MC3-LNP-GNPs without porphyrin-lipids as a control. In absence of porphyrin-lipids, the GNPs stably remained in endosomal structures with clear membrane integrity after 1.5 J/cm^2 light irradiation (Figure S17), further confirming that porphyrin-lipid is a key component for light-induced endosomal membrane disruption.

Overall, the observations of GAL9 recruitment and GNP release into cytosol upon light irradiation provided direct evidence for membrane damage during porphyrin-LNP mediated LASER. Along with previous finding regarding porphyrin-lipid translocation to endocytic organelle membranes, the mechanisms of ROS-induced endocytic membrane damage via LASER have been clearly elucidated.

Determination of siRNA Endosomal Escape Efficiency.

After providing qualitative evidence of LASER, we next established a 3D real-time live cell imaging method to quantitatively evaluate siRNA endosomal release in LASER. As shown in Figure 5a, 3D microscopy images of porphyrin-LNP treated cells were processed by Imaris to reconstruct organelles and cell structures. Spatial parameters of interest (*i.e.*, fluorescent intensity sum in cytosols versus organelles) were quantified and masked images displaying only siRNA signals from cytosols were created. We applied this analysis pipeline to quantify the relative levels of siRNA in the cytosol following light irradiation ranging in duration from 15 s to 1 min (Figure 5b–f). Correlative enhancement of the FAM-siRNA signal in the cytosol was observed, with cytosolic FAM fluorescence intensity sums enhanced by 30–90% as compared to those before irradiation (Figure 5b,c). Upon further irradiation up to 2 min, the level of augmentation dropped slightly to 70%. Interestingly, after short irradiation, the FAM-siRNA signal in endocytic organelles was also increased by a level of 47% and 20% at 15 and 30 s post irradiation, respectively, with a marked organelle color change from predominantly magenta (prelaser) to white (postlaser) (Figure 5b,d). The organelle color change is also consistent with our previous observation after 30 s irradiation (Figure 3a magnified view). These quantitative data strongly suggest FAM-siRNA fluorescence activation occurred inside the endocytic organelles due to ROS-facilitated LNP dissociation before its subsequent escape into the cytosol. Upon longer irradiation times (1 and 2 min), siRNA continued to escape from endocytic organelles, as evidenced by the decreasing FAM-siRNA signal in endocytic organelles by 20% and 27% post irradiation. This “activation first–then release” pattern of the siRNA signal in endocytic organelles revealed two different release stages involved in LASER: at relatively low light fluence, porphyrin-generated ROS facilitated (1) preliminary endosomal escape of a small portion of FAM-siRNA (already dissociated from LNPs) into cytosols and (2) enhanced LNP dissociation which relieved some FAM-siRNA from a densely packed status

in the core of LNP, as evidenced by the strong FAM fluorescence recovery. Upon relatively higher fluence, ROS-induced endocytic membrane disruption became the dominant effect therefore diminishing siRNA signal in the organelles due to their endosomal escape. Irradiation over 2 min could cause cellular membrane damage which decreases cytosolic siRNA signal as siRNA efflux from cells. The “activation first–then release” pattern was also supported by calculating % FAM-siRNA signal change of organelle to cell volume ratio (Figure 5e). The initial increased ratio at 15 and 30 s post irradiation suggested FAM-siRNA activation in the organelles while the decreased ratio at 1 and 2 min post irradiation indicated endocytic organelle disruption and FAM-siRNA migration into cytosol. Pearson’s colocalization coefficient R between FAM-siRNA signal and porphyrin-lipid signal in the whole 3D data volume exhibited no significant change 15 or 30 s post irradiation, whereas a significant decrease of Pearson’s R was noticed at 1 min (0.65 to 0.52) and 2 min (0.58 to 0.43) post irradiation (Figure 5f). The colocalization profile is matched with the two-step FAM-siRNA release process: FAM-siRNA activation within the endocytic organelles followed by their release into the cytosol.

After establishing the relative cytosolic changes of siRNA abundance in relation to the LASER approach, we next investigated the absolute siRNA concentration in cytosols using the pipeline outlined in Figure S18a. Briefly, for images of interest, after subtracting the background signal in the FAM-siRNA channel, the cytosolic FAM-siRNA concentration was calculated from a standard curve of FAM-siRNA concentration against intensity per voxel in the cytosols (Figure S18b–e). The cytosolic FAM-siRNA concentration was quantified to be 60–80 nM before irradiation and increased to 75–125 nM post irradiation (Figure S18f). Next, the number of siRNA copies in the cytosol was calculated using 5000 femtoliters (fL) as the total cytosol volume of a cell.⁴⁰ The mean cytosolic siRNA copies were calculated to be 2.1×10^5 per cell at 6 h incubation time. Post 15 s and 1 min light irradiation, the mean siRNA copies in the cytosol increased to 2.3 and 4.8×10^5 per cell, respectively (Figure 5g).

Next, we quantified the porphyrin-LNP cell uptake as an alternative method to determine the total siRNA copies in both cytosols and organelles (the detailed method is described in Materials and Methods and Figure S19). A time-dependent porphyrin-LNP-siRNA intracellular uptake profile was observed after incubating cells with porphyrin-LNP for 1, 3, and 6 h. After 6 h uptake, 2.3×10^7 siRNA copies were taken up by each cell (Figure 5h; eqs 1 and 2). In combination with cytosolic siRNA copy number (Figure 5g), siRNA endosomal escape efficiency was calculated to be 0.8–1.0% before irradiation (Figure 5i; eq 3), consistent with the 1–2% siRNA endosomal escape efficiency from LNPs as reported in the literature.⁷ Notably, the mean endosomal escape efficiency doubled from 1.0% to 2.1% at 1 min post irradiation, indicating a 2-fold increase in copies of cytosolic siRNA. As the FAM-siRNA signal in endocytic organelles originated from FAM-siRNA that was unquenched, this suggests the LASER strategy can sufficiently enable endosomal escape of siRNAs that are already dissociated from the LNPs. However, the lack of siRNA copies present in the

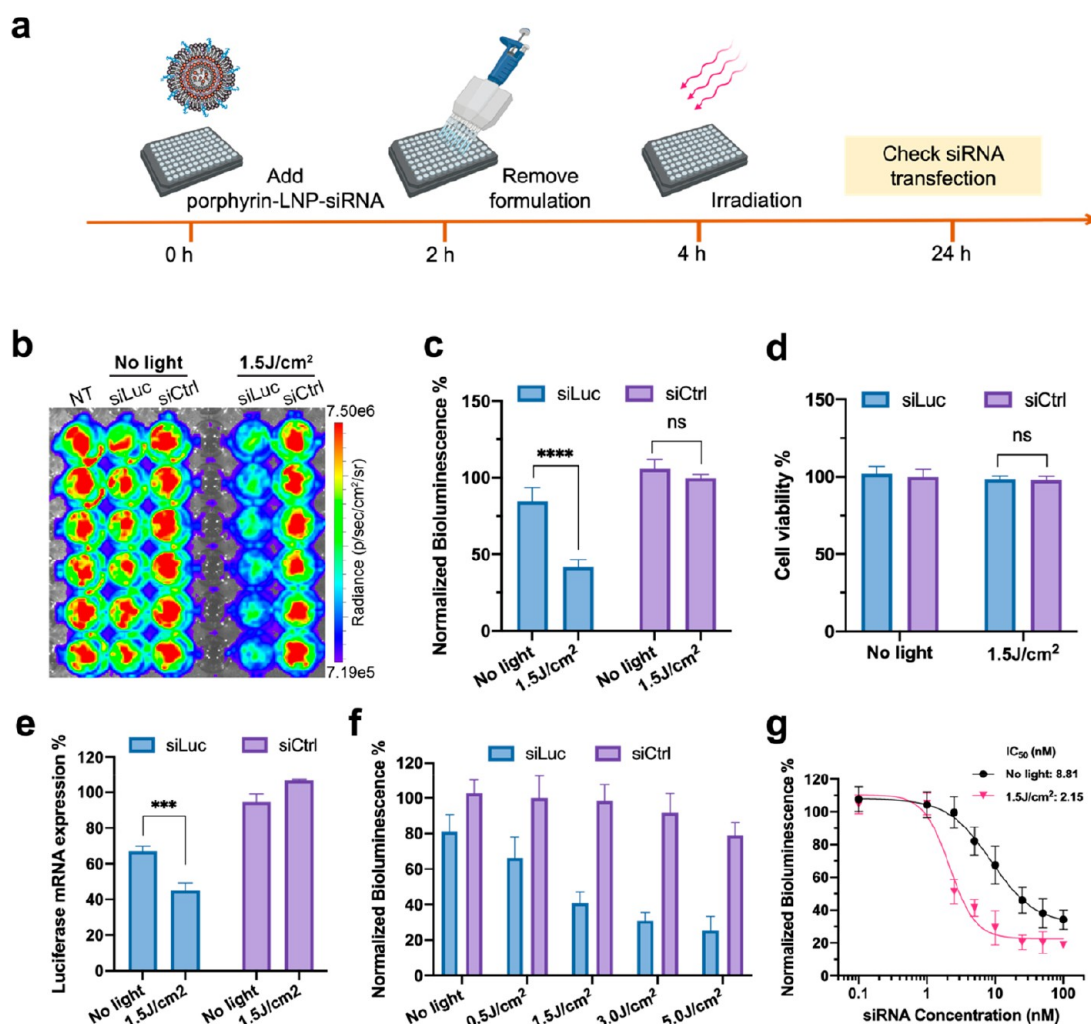


Figure 6. Influence of LASER on porphyrin-LNP *in vitro* transfection efficacy. (a) Schematic illustration of experimental design. (b) Representative bioluminescent image of PC3-Luc6 cells after porphyrin-LNP and light treatment. Porphyrin-LNPs were given a siRNA dose of 5 nM per well. (c) Normalized bioluminescence intensity and (d) cell viability of PC3-Luc6 cells after porphyrin-LNP and light treatments. **** $p < 0.0001$ (e) Luciferase mRNA expression in PC3-Luc6 cells after porphyrin-LNP incubation at 10 nM siRNA dose and light treatment. *** $p < 0.005$ (f) Influence of light dose on porphyrin-LNP transfection potency. Porphyrin-LNPs were given at siRNA dose of 5 nM per well. (g) Dose–response curve of porphyrin-LNP-siLuc when treated with PC3-Luc6 cells with (Red triangle) and without (Black dot) irradiation at 1.5 J/cm². Data are presented as means \pm standard deviation ($n = 3$).

cytosols implied a significant proportion of siRNA remained entrapped in the organelles despite of endosomal membrane damage. This could be a likely outcome if the siRNA fails to dissociate from LNPs, and the siRNA-lipid complex hinders the endosomal escape process even upon membrane disruption.⁴¹ These observations provided insight into the LASER mechanisms and also indicated the potential challenges that arise from the lack of LNP dissociation for RNA endosomal escape. Therefore, we anticipate an enhanced siRNA endosomal escape via LASER and porphyrin-LNP if dissociation between LNP and siRNA can be further improved.

LASER Improves siRNA *In Vitro* Transfection Potency.

After unveiling mechanisms of porphyrin-LNP-mediated LASER through imaging approaches, we next investigated the influence of LASER on siRNA transfection potency via *in vitro* luciferase knockdown experiments. The experiment flow is outlined in Figure 6a. The PC3-Luc6 cells were treated with porphyrin-LNP-siLuc at 5 nM siRNA concentration and irradiated at a light dose of 1.5 J/cm². The light irradiation

significantly enhanced luciferase knockdown in PC3-Luc6 cells by 4-fold from 15% (without light) to 58% (light-treated), while no significant knockdown was noticed for the porphyrin-LNP-siCtrl treated group with or without light irradiation (Figure 6b,c). Importantly, no cytotoxicity was observed for all treatment groups (Figure 6d). These data support that light irradiation eventually enhanced siRNA transfection efficacy without causing cytotoxicity. We further validated siRNA knockdown efficacy at the luciferase mRNA expression level using RT-qPCR experiments (Figure 6e). In concordance with bioluminescence measurements, cells treated with porphyrin-LNP-siLuc and a light dose of 1.5 J/cm² exhibited improved luciferase mRNA knockdown from 33% (without light) to 55% (light-treated), whereas cells treated with porphyrin-LNP-siCtrl again showed negligible knockdown with or without light treatment. This suggests that more siRNA was released into the cytosol after irradiation which led to more effective mRNA silencing. Next, we performed both light dose and siRNA dose escalation study to determine the siRNA knockdown efficacy by

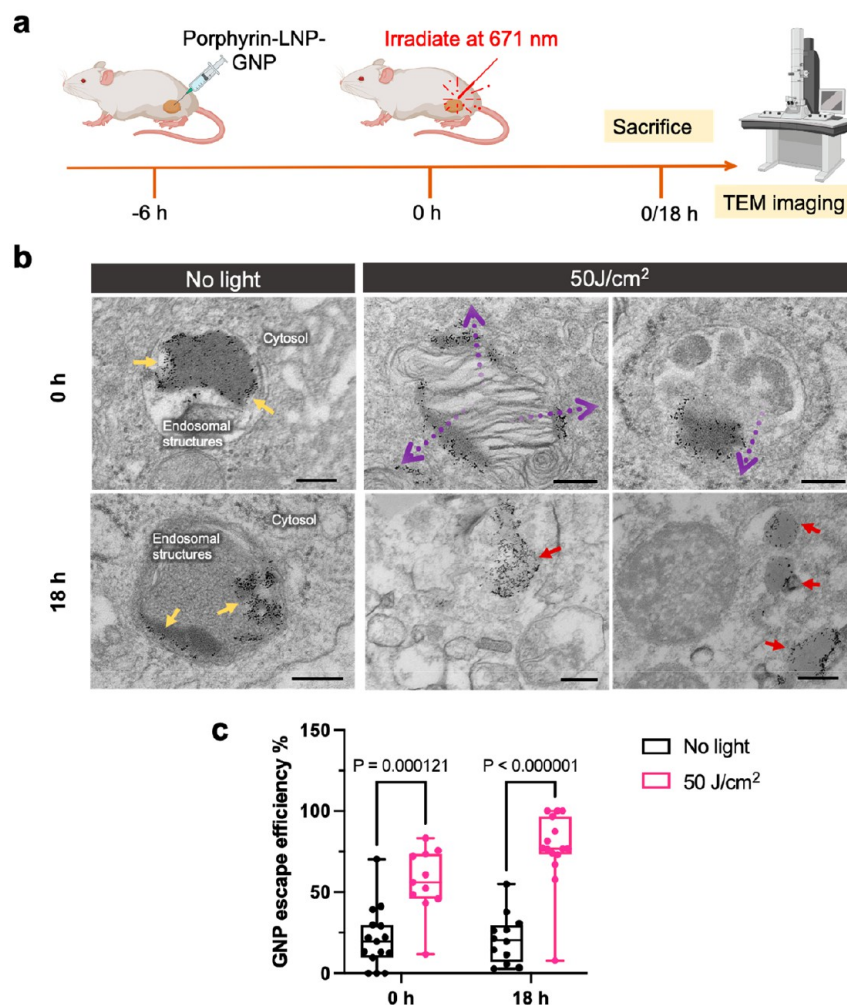


Figure 7. Visualization of GNP subcellular localization *in vivo*. (a) Schematic illustration of experimental design: mice bearing subcutaneous PC3-Luc6 tumors were intratumorally injected with porphyrin-LNP-GNP. After 6 h, mice were treated with or without 50 J/cm² irradiation at 671 nm. Then mice were sacrificed immediately or 18 h later. Tumors were collected and prepared for TEM imaging. (b) Representative TEM images of endosomal structures from tumors treated with and without irradiation and dissected at given time points. Yellow arrows, trapped GNPs inside organelles; purple arrows, GNPs that were escaping from the organelles; red arrows, free GNPs that distributed in cytosols. Scale bar: 200 nm. (c) Quantification of GNP endosomal escape efficiency from tumors treated with and without light irradiation with dissection at the indicated time points post irradiation. Each data point represents quantification results from one cell. *t* test was performed to calculate the statistical significance.

porphyrin-LNP-siLuc. We observed that increasing the light dose from 0.5 J/cm² to 3 J/cm² resulted in further luciferase knockdown from 34% to 69%, respectively (Figure 6f). The porphyrin-LNP-siCtrl treated cells did not exhibit luciferase knockdown under a light dose of 3 J/cm². However, further increasing the light dose to 5 J/cm² resulted in significantly reduced cell viability (~50%) as a consequence of the PDT effect (Figure S20). To maximize the benefit from LASER while minimizing the PDT impact on cell viability, 1.5 J/cm² was selected as the optimized light dose. Using 1.5 J/cm², we further investigated siRNA dose-dependent knockdown. The half-maximal inhibition concentration (IC₅₀) of porphyrin-LNP-siLuc and Onpattro-LNP with and without light treatment was determined. While no significant change of IC₅₀ was observed for Onpattro-LNP when light was applied (Figure S21), A 4-fold decrease of IC₅₀ from 8.81 to 2.15 nM was achieved for porphyrin-LNP-siLuc by LASER (Figure 6g). Significantly, >10-fold improvement was observed under a low siRNA dose (2.5

nM) by 1.5 J/cm² light activation, resulting in increased knockdown efficiency from <3% to ~50%. Of note, when siRNA dose decreased from 50 to 2.5 nM, porphyrin-lipid concentration also decreased 20-fold from ~1 to 0.05 μM, which suggests the feasibility to apply LASER even at low porphyrin-lipid dose. Since the porphyrin-LNP-based LASER approach enabled higher transfection efficacy at lower siRNA concentration, the siRNA dose needed to achieve potent mRNA silencing can be significantly reduced. Overall, the *in vitro* luciferase silencing assay using LASER supported our previous imaging findings that light-irradiation significantly improved siRNA endosomal escape and available siRNA copies in cytosol, which ultimately translated to enhanced RNAi therapeutic efficacy with a 4-fold decrease of siRNA IC₅₀.

Improving Endosomal Escape with Porphyrin-LNP *In Vivo*. To validate LASER strategy using porphyrin-LNP *in vivo* (Figure 7), mice bearing subcutaneous PC3-Luc6 tumors were injected intratumorally with porphyrin-LNP-GNP (20 μg

porphyrin-lipid) prior to 50 J/cm² laser irradiation at the tumor site with a drug-light interval (DLI) of 6 h. Subsequently, tumors were extracted either immediately or at 18 h post-treatment to evaluate the rapid and delayed changes on endosomal membrane integrity through TEM imaging (Figure 7a). As shown in Figures 7b and S22, for control mice receiving no light irradiation, the GNPs were mainly observed in endosomal structures (yellow arrows) at both time points, consistent with *in vitro* observations on control cells. Notably, GNPs were complexed with electron-dense components (possibly ionizable lipids),^{42,43} which could indicate GNPs-lipid complexes even after LNP dissociation in the endocytic organelles. On the other hand, for light-irradiated tumors (Figures 7b and S23), GNPs-lipid complexes were found to migrate from endosomal structures to cytosols immediately after irradiation (purple arrows). The endosomal membrane's integrity also appeared compromised around the areas where the GNPs-lipid complexes were located. This indicated the possible role of porphyrin-lipids in the darker regions that it induced initial membrane disruption upon exposure to light. In comparison, for the tumors which were dissected 18 h later after irradiation, GNPs started to show more pronounced cytosolic distributions (red arrows), which were not enclosed by any membrane structures, indicating a more complete release from endosomal structures as a result of membrane disruption. We next quantified GNP subcellular localization in the organelles versus in the cytosol and calculated GNP endosomal escape efficiency (Figure 7c, detailed methods in Figure S24). Light irradiated tumors showed significantly higher average GNP endosomal escape efficiency at both 0 h (56.7%) and 18 h (76.8%) after light treatment compared to corresponding nonirradiated tumors (21.5% and 21.3%, respectively). The 2.5–3.5-fold increase in GNP endosomal release efficiency after applying illumination is comparable to our *in vitro* quantification using a fluorescence method (Figure S5). Together, the visualization and quantification of GNP subcellular localization provided early evidence that porphyrin-LNP and LASER can promote endocytic membrane disruption and enhance its cargo release into the cytosol *in vivo*.

CONCLUSIONS

In summary, this study demonstrates the feasibility and possible mechanisms of a Light-Activated siRNA Endosomal Release (LASER) approach using porphyrin-LNPs. Porphyrin-LNPs were established by replacing helper lipids from the clinically used Onpatro formulation with porphyrin-lipids. Incorporating porphyrin-lipids enabled LNPs to generate ROS upon NIR light irradiation. We investigated the mechanisms of LASER and revealed porphyrin-lipids translocation from the LNP to the endocytic organelle membranes in the endocytosis process, thereby generating membrane-specific ROS upon light irradiation. The porphyrin-LNP-mediated LASER approach significantly improves siRNA endosomal escape by facilitating both endosomal membrane disruption and LNP dissociation. We discovered a positive correlation between siRNA endosomal escape efficiency and transfection efficacy *in vitro* mediated by LASER. Lastly, we demonstrated the effect of LASER to enhance the cytosolic delivery of GNP *in vivo*. We believe that porphyrin-LNPs and LASER have great potential to improve transfection efficacy of RNA therapeutics by addressing barriers that hinder endosomal escape. This study would provide insights for the rational design of light-activatable LNP systems, and it offers a simple approach toward the improvement of LNP-based RNA therapeutics.

MATERIALS AND METHODS

Materials. 1,2-Distearoyl-*sn*-glycero-3-phosphocholine (DSPC), cholesterol, and 1,2-dimyristoyl-*rac*-glycero-3-methoxy(poly(ethylene glycol))-2000 (DMG-PEG2000) were purchased from Avanti Polar Lipids (Alabaster, AL, USA). DLin-MC3-DMA was purchased from Nanosoft Polymers (NC, USA). Porphyrin-lipid was synthesized by the previously reported methods.²⁶ D-Luciferin (potassium salt) was purchased from PerkinElmer. mCherry-GAL9 was a gift from Dr. Alan Sabirsh (Addgene plasmid # 166689).

Small Interfering RNA. Luciferase targeting siLuc and scrambled siCtrl were both purchased from Horizon Discovery (USA). siLuc: sense, 5'-GAU UAU GUC CGG UUA UGU AdTsdT-3'; antisense, 5'-UAC AUA ACC GGA CAU AAU CdTsdT-3'. FAM-siLuc: sense, 5'-FAM-GAU UAU GUC CGG UUA UGU AdTsdT-3'; antisense, 5'-UAC AUA ACC GGA CAU AAU CdTsdT-3'. siCtrl: sense, 5'-UUC UCC GAA CGU GUC ACG UdTsdT-3'; antisense, 5'-ACG UGA CAC GUU CGG AGA AdTsdT-3'.

Preparation of Porphyrin-LNP. Porphyrin-LNPs were prepared using a microfluidic rapid mixing method as previously reported.³³ Unless otherwise stated, lipids were mixed in ethanol at a molar ratio of 50/10/38.5/1.5 (DLin-MC3-DMA/Porphyrin-lipid/Cholesterol/DMG-PEG₂₀₀₀). siRNA was dissolved in 25 mM sodium acetate buffer (pH = 4.0). The two phases were mixed through herringbone microfluidic chips (microfluidic ChipShop, Germany) at a volume flow rate ratio of 3:1 (aqueous to ethanol) and total flow rate of 10 mL/min. The mixed solution was dialyzed against PBS 7.4 overnight. Afterward LNPs were concentrated to 1–10 mg/mL total lipid concentration based on need in experiments using ultracentrifuge filters (Amicon, Sigma-Aldrich) and passed through 0.22 μm filter before use.

Preparation of Porphyrin-LNP-GNP. The porphyrin-LNP-GNP was prepared by combining 50 mol % DLin-MC3-DMA, 10 mol % Porphyrin-lipid, 38.5 mol % cholesterol, and 1.5 mol % DMG-PEG2000 into a lipid mixture with a final lipid concentration of 10 mM in ethanol. The organic phase was subsequently mixed with PELCO NanoXact 5 nm T.Cap GNP (Ted Pella, Inc., Redding, CA) in 25 mM NaOAc pH4 buffer (GNP/lipid ratio: 3.3 × 10¹³ particles/μmol) through a T-junction mixer (total flow rate: 20 mL/min, ratio of 1:3 v/v organic/aqueous). The mixture was dialyzed against at least 1000-fold volumes of PBS overnight to remove untrapped GNPs and ethanol. The particles were then sterile filtered and concentrated to ~10 mg/mL lipid using an Amicon Ultracel 100 kDa MWCO centrifugal unit (Millipore, Billerica, MA). The total lipid concentration of the resulting LNP was calculated from cholesterol measurement using the Cholesterol E Total-Cholesterol assay (Wako Diagnostics, Richmond, VA). The GNP concentration of the Porphyrin-LNP-GNP was determined from a standard curve in Triton X-100 at 520 nm absorbance and quantified using a Spark microplate reader (TECAN, Switzerland).

In Vitro Characterization of Porphyrin-LNP. The hydrodynamic size and poly dispersity of porphyrin-LNPs were characterized using a Zetasizer Nano ZS (Malvern Instruments). The morphology of porphyrin-LNP were confirmed by TEM and cryo-EM. Absorbance and fluorescence spectrum of Porphyrin-LNPs were collected on a UV-vis spectrophotometer Cary 50 (Agilent, Mississauga, ON) and Fluoromax fluorometer (Horiba Jobin Yvon, USA) respectively. siRNA concentration and encapsulation efficiency were measured by Quant-it RiboGreen RNA Assay based on manufacturer's protocol (Thermo-fisher). Briefly, LNPs were diluted in equal volumes of Tris-EDTA (TE) buffer or 2% Triton X-100 in TE buffer. Next, RiboGreen reagent was added into each sample wells and incubated at 37 °C for 15 min before measuring its fluorescence intensities (Ex/Em: 480/520 nm). Fluorescence signal from TE buffer treated samples (F_{TE}) represents unencapsulated siRNA while fluorescence signal from TX-100 treated samples (F_{TX}) represents total siRNA. siRNA encapsulation efficiency can be determined as

$$\text{encapsulation \%} = \frac{F_{TX} - F_{TE}}{F_{TX}} \times 100\%$$

siRNA release from LNP was also determined by RiboGreen assay. Briefly, LNPs were incubated with EMEM+10%FBS or PBS buffer at varying pH at siRNA concentration of 1 $\mu\text{g}/\text{mL}$. The amount of siRNA encapsulated in LNP was monitored over time during incubation at 37 $^{\circ}\text{C}$ for 24 h.

Singlet Oxygen Measurement. Singlet oxygen ($^1\text{O}_2$) generation of porphyrin-LNPs was measured using singlet oxygen sensor green (SOSG, Invitrogen) assay. Briefly, SOSG solution was freshly prepared in methanol (5 mM) and diluted with PBS before mixing with porphyrin-LNP samples (1 μM porphyrin), to have a final SOSG concentration of 10 μM . Samples were irradiated with a free-space laser (LaserGlow Technologies) at 671 nm with 50 mW/cm^2 irradiance to achieve light doses from 0.5 to 5 J/cm^2 . Afterward, SOSG fluorescence was measured by a CLARIOstar plate reader (BMG LABTECH) at 488 nm excitation and 525 nm emission.

Cryo-EM Image Acquisition. Porphyrin-LNP-siRNA and porphyrin-LNP-GNP were imaged with an FEI Tecnai G20 transmission electron microscope (FEI, Hillsboro, OR) as previously described.⁴² LNPs were concentrated to approximately 15–20 mg/mL of total lipid. The LNPs sample preparation and image acquisition were performed by the UBC Bioimaging Facility (Vancouver, BC).

Cell Culture. PC-3M-luc-C6 cells (PC3-Luc6) were purchased from Caliper Life Sciences and cultured in Eagle's Minimum Essential Medium (supplemented with 10% FBS). The other cell lines were purchased from ATCC and cultured as follows: PANC-1 (DMEM+10% FBS); 4T1 (RPMI-1640 + 10%FBS); A549 (RPMI-1640 + 10%FBS); SKOV-3 (McCoy's 5 + 10%FBS). All the cell lines were maintained at 37 $^{\circ}\text{C}$ under 5% CO_2 .

In Vitro Luciferase Knockdown. PC3-Luc6 cells were seeded at 4000 cells per well into 96-well plates for 48 h. Then cells were incubated with LNPs at different siRNA concentration overnight (unless otherwise stated), after which the cells were washed twice with culturing medium and the wells were replaced with medium that contains 0.05 mg/mL alamarBlue (Invitrogen). The cells were incubated for an additional 2 h, and the cell viability was calculated through measuring fluorescence emission of the alamarBlue assay using a CLARIOstar microplate reader (excitation of 540/8 nm and emission of 590/8 nm). Luciferase expression of PC3-Luc6 on the same plate was evaluated through bioluminescence, where 5 μL of D-luciferin solution (25 mM) was added into each well (100 μL medium) and bioluminescence was collected with an IVIS Spectrum *In vivo* Imaging System (PerkinElmer). The bioluminescence intensity of each well was further normalized by its viability before analysis.

For laser-involved luciferase knockdown experiments, once cells were incubated with porphyrin-LNP for 2 h, cells were washed twice with culturing medium and replenished with fresh medium for a subsequent 2 h incubation. Cells were then irradiated with a 671 nm laser (spot area: 0.71 cm^2) at 30 mW/cm^2 irradiance to achieve light dose from 0.5 J/cm^2 to 5 J/cm^2 . Following irradiation, cells were further incubated for 20 h, after which their viability and luciferase expression were measured in a same way as described above.

Reverse Transcription-Quantitative Real-Time PCR. Total RNA of cells after treatments was extracted using TRIzol reagent (Invitrogen Life Technologies, Inc.) and RNeasy Mini kit (Qiagen). cDNA was next synthesized using High-Capacity cDNA Reverse Transcription Kit (ThermoFisher). For cDNA amplification, PowerUp SYBR Green Master Mix (ThermoFisher) and the following primers were used: GAPDH (sense: 5'-CAT GAG AAG TAT GAC AAC AGC CT-3'; antisense: 5'-AGT CCT TCC ACG ATA CCA AAG T-3'); luciferase (sense: 5'-ATT ACA CCC GAG GGG GAT GA-3'; antisense: 5'-CCA GAT CCA CAA CCT TCG CT-3'). The comparative cycle threshold (Ct) method was used to calculate relative abundance of luciferase mRNAs (GAPDH mRNA as internal control). Each assay was conducted in triplicate.

Confocal Imaging of Light-Induced siRNA Endosomal Escape. For confocal imaging studies, cells were seeded into 8-well coverglass-bottom chambers (Nunc LabTek, Sigma-Aldrich, Rochester, NY) at a cell-seeding density of 2×10^4 cells per well. After 48 h, porphyrin-LNPs load with FAM-siRNA were added at a concentration of 4 μM (based on porphyrin) and incubated for given

time periods. Cells were then washed twice with culturing medium before imaging. Confocal microscopy was performed in the Advanced Optical Microscopy Facility, University Health Network. Fluorescence images were captured by stimulated emission depletion (STED) microscopy (Leica, Germany) using a 63 \times oil objective lens. Customized filter settings were used to collect signals from porphyrin-lipid (excitation: 633 nm; emission: 670–765 nm, laser power 1–5%) and FAM-labeled siRNA (excitation: 488 nm; emission: 507–580 nm, laser power 30–60%). During irradiation, porphyrin-lipid was irradiated at 660 nm and the laser power was raised to 100% for given time intervals. Laser power and detector gain adjustment were kept consistent before and post laser irradiation. Specifically, images for porphyrin-lipid membrane localization were captured with 100% laser power and 10% detector gain to obtain the highest imaging resolution. For Pearson's correlation coefficient (PCC), it is calculated by the following formula for a typical image consisting of red and green channels:⁴⁴

$$\text{PCC} = \frac{\sum_i (R_i - \bar{R}) \times (G_i - \bar{G})}{\sqrt{\sum_i (R_i - \bar{R})^2 \times \sum_i (G_i - \bar{G})^2}}$$

where R_i and G_i refer to the intensity values of the red and green channels, respectively, of pixel i , and \bar{R} and \bar{G} refer to the mean intensities of the red and green channels, respectively, across the entire image. PCC values range from 1 for two images whose fluorescence intensities are perfectly, linearly related, to -1 for two images whose fluorescence intensities are perfectly, but inversely, related to one another. Specifically, for the images analyzed in our study, images were processed using Fiji software and Coloc 2 plugin was used to perform PCC calculation following the principle stated above.

Endosomal Organelle Colocalization. PC3-Luc6 cells were seeded into 8-well coverglass-bottom chambers and transfected with CellLight Early Endosomes-RFP and Late Endosomes-RFP BacMam 2.0 kits (Molecular Probes) for Rab5a (EE marker) and Rab7A (LE marker). Lysosomes were stained using LysoTracker Red DND-99 (ThermoFisher) based on manufacturer's protocol. PC3-Luc6 cells were incubated with porphyrin-LNP at a porphyrin concentration of 4 μM for 1, 3, and 6 h. Cells were then washed twice with culture medium before imaging though confocal microscopy.

Visualization of GAL9 Recruitment after Laser. PC3-Luc6 cells were seeded into 8-well coverglass-bottom chambers at a cell-seeding density of 2×10^4 cells per well and transfected with plasmid encoding mCherry-galectin-9 (Addgene # 166689) through Lipofectamine 3000 (ThermoFisher) for 2 days before use. Porphyrin-LNPs loaded with FAM-siRNA were then added at a concentration of 4 μM (based on porphyrin) and incubated for 6 h with the cells. Cells were washed twice with culture medium before being imaged by confocal microscopy. Customized filter settings were used to collect signal from porphyrin-lipid (ex: 633 nm; em: 670–765 nm), FAM-labeled siRNA (ex: 488 nm; em: 507–580 nm), and mCherry-Gal9 (ex: 561 nm; em: 575–649 nm). During irradiation, the laser power of 660 nm was raised to 100% for given time intervals. Laser power and detector gain adjustment were kept consistent before and post laser irradiation.

Visualization of In Vitro GNP Subcellular Localization after Laser. PC3-Luc6 cells were seeded into T-25 flasks at a cell-seeding density of 4×10^5 cells per flask. After 48 h, cells were treated with porphyrin-LNP-GNP at a final porphyrin concentration of 8 μM for 24 h. For MC3-LNP-GNP, it was added at same GNP concentration as porphyrin-LNP-GNP. Next, the cells were washed three times with PBS before subsequent trypsinization. Cells were collected and spined down at 1000 rpm for 5 min, after which the supernatant was removed, and the cells were resuspended in 2 mL cell culture medium. Next, half of the suspending cells were placed in 96-well plate at 200 μL per well and irradiated with a free-space laser at 671 nm with a 30 mW/cm^2 irradiance to achieve light dose of 1.5 J/cm^2 . Subsequently, both irradiated and unirradiated cells were collected and spined down to form cell pellets in 1.5 mL Eppendorf tube. The supernatant was removed, and the cells were fixed in 2.5% glutaraldehyde + 2% PFA in 0.1 M sodium cacodylate buffer before subsequent TEM grid preparation and imaging with a Hitachi HT7800 transmission electron

microscope (Nanoscale Biomedical Imaging facility, Peter Gilgan Centre for Research and Learning, Toronto).

Quantitative Analysis of siRNA Endosomal Escape. To get quantitative imaging results from fluorescent images, fluorescent images of PC3-Luc6 after treatment with porphyrin-LNP were captured across Z-stacks (20 μm , step = 1 μm). Then the 3D images were processed by Imaris 9.9 (Oxford Instruments) to reconstruct punctate organelles and surface structures of all the cells: briefly, organelles were identified using “surface” object (Surface Grain Size = 0.300 μm , Diameter of Largest Sphere = 2.00 μm , Manual Threshold Value = 10) while cell membranes were identified using “cell” object (Cell Smooth Filter Width = 1.00 μm , Cell Background Subtraction Width = 40.0 μm , Cell Manual Threshold = 4.000, “Cell Number of Voxels” above 2000), both based on fluorescent signal from FAM-siRNA channel. After organelle and cell structures were identified, masked FAM-siRNA signal was generated by subtracting organelle-originated FAM signals from each cell in the original FAM channel. Subsequently, statistics of interests were extracted by Imaris and analyzed to generate quantitative results.

For absolute FAM-siRNA concentration quantification in cytosol, FAM-siRNA fluorescence intensity standard curve was first established in 3D confocal imaging data sets using cell culture medium containing only FAM-siRNA. The background signal in the FAM-siRNA channel was measured using porphyrin-LNP (no FAM label) samples under same imaging conditions. To quantify the FAM-siRNA concentration in unknown samples, the background was subtracted first, followed by calculating siRNA concentration in cytosols using the established FAM-siRNA fluorescence standard curve.

Quantitative Cell Uptake and Determination of siRNA Endosomal Escape Efficiency. Briefly, cells were seeded into 96-well plates. Then 48 h later, porphyrin-LNPs were added at a concentration of 4 μM (based on porphyrin) and incubated for given time periods. Afterward, the cells were washed twice with culturing medium and the wells were replaced with medium that contains 0.05 mg/mL alamarBlue (Invitrogen) for viability measurement. Then medium was removed again and replaced with 200 μL /well DMSO solution to fully digest the cells and unquench any porphyrin-lipids that were uptaken into cells, followed by measurement of porphyrin fluorescence using plate reader. Cell counts in each well were calculated by fitting alamarBlue assay readout to cell counts standard curve created also from alamarBlue assay.⁴⁵ For cell counts standard curve, it is prepared by seeding cells into 96-well plate at gradient density, after overnight incubation, cells were added with alamarBlue and measured fluorescence intensity. Porphyrin amount was quantified by fitting porphyrin fluorescence to its standard curve prepared in DMSO. Combining these two data, total porphyrin-lipid amount per cell was obtained as follows:

$$\begin{aligned} & \text{porphyrin amount per cell} \\ &= \frac{\text{porphyrin concentration} \times \text{DMSO digestion volume}}{\text{total cell counts per well}} \end{aligned} \quad (1)$$

Since siRNA and porphyrin-lipids were at a fixed ratio in LNPs, which is determined by siRNA concentration and porphyrin-lipid concentration in the LNP. siRNA amount per cell can be further calculated as follows:

$$\begin{aligned} & \text{siRNA amount per cell} \\ &= \frac{\text{porphyrin amount per cell} \times \text{siRNA concentration}}{\text{porphyrin concentration}} \end{aligned} \quad (2)$$

For FAM-siRNA endosomal escape efficiency calculation, the number of cytosolic siRNA copies per cell was calculated using cytosolic FAM-siRNA concentration and 5000 fL as the total cytosol volume of a cell.⁴⁰ Next, the number of total siRNA copies per cell was determined by quantitative cell uptake experiment as described above. Then FAM-siRNA endosomal escape efficiency can be calculated as follows:

$$\begin{aligned} \text{escape efficiency \%} &= \frac{\text{cytosolic siRNA copy number}}{\text{total siRNA copy number}} \times 100\% \end{aligned} \quad (3)$$

Xenograft Mouse Models. All animal studies were approved and conducted in compliance with the University Health Network Animal Resources Centre guidelines. For the generation of subcutaneous tumor xenografts, athymic male nude mice under general anesthesia were inoculated with 3×10^6 PC3-Luc6 cells in 100 μL PBS into the right flank. Tumor growth was monitored using electronic calipers.

Visualization of *In Vivo* GNP Subcellular Localization after Laser. For porphyrin-LNP-GNP subcellular localization studies *in vivo*, once tumors reached 100 mm³, mice bearing PC3-Luc6 subcutaneous tumors ($n = 3$ for each group) were injected intratumorally with 20 μg (based on porphyrin-lipid) of porphyrin-LNP-GNP. After 6 h, the irradiated group of mice was put under general anesthesia using isoflurane, and tumors were irradiated with a 671 nm PDT laser (Laserglow Technologies, Toronto, ON, Canada) at a fluence rate of 50 mW/cm² and a total light dose of 50 J/cm². After irradiation, half of the mice were sacrificed immediately to evaluate the rapid effect of irradiation on membrane integrity and GNP localization while the other half of the mice were sacrificed 18 h later to evaluate the delayed effect. Tumors were collected after dissection and fixed in 2.5% glutaraldehyde + 2% PFA in 0.1 M sodium cacodylate buffer for subsequent TEM grids preparation and imaging. For GNP endosomal escape efficiency quantification, Fiji was used to analyze the images. Detailed image processing example is provided in Figure S24.

ASSOCIATED CONTENT

Supporting Information

The Supporting Information is available free of charge at <https://pubs.acs.org/doi/10.1021/acsnano.2c10936>.

Influence of porphyrin-lipid molar ratio on LNP transfection, singlet oxygen generation and emission spectrum of disrupted porphyrin-LNP, porphyrin-LNP size at varying pH and irradiation by DLS and TEM, colloidal and optical stability of porphyrin-LNP, intracellular colocalization between porphyrin-LNP and organelles, confocal images of cells treated with control LNPs, cryo-EM images of porphyrin-LNP-GNP, TEM images of cells treated with MC3-LNP-GNP, quantitation of porphyrin-LNP cellular uptake profile and cytosolic siRNA concentration, cell viability upon different dose of light irradiation, dose–response curve of cells treated by Onpattro LNP, TEM images of tumor endosomal structures after porphyrin-LNP-GNP treatment and GNP subcellular localization quantification (PDF)

AUTHOR INFORMATION

Corresponding Authors

Juan Chen – Princess Margaret Cancer Center, University Health Network, Toronto, Ontario M5G 1L7, Canada; Email: juan.chen@uhnresearch.ca

Gang Zheng – Institute of Medical Science, University of Toronto, Toronto, Ontario M5G 1L7, Canada; Princess Margaret Cancer Center, University Health Network, Toronto, Ontario M5G 1L7, Canada; Department of Medical Biophysics, University of Toronto, Toronto, Ontario M5G 1L7, Canada; orcid.org/0000-0002-0705-7398; Email: gang.zheng@uhnres.utoronto.ca

Authors

Yulin Mo – Institute of Medical Science, University of Toronto, Toronto, Ontario M5G 1L7, Canada; Princess Margaret Cancer Center, University Health Network, Toronto, Ontario M5G 1L7, Canada

Miffy H. Y. Cheng – Department of Biochemistry and Molecular Biology, University of British Columbia, Vancouver,

British Columbia V6T 1Z3, Canada; orcid.org/0000-0002-0261-4642

Andrew D'Elia – Princess Margaret Cancer Center, University Health Network, Toronto, Ontario M5G 1L7, Canada

Katie Doran – Princess Margaret Cancer Center, University Health Network, Toronto, Ontario M5G 1L7, Canada; orcid.org/0000-0002-4804-1309

Lili Ding – Princess Margaret Cancer Center, University Health Network, Toronto, Ontario M5G 1L7, Canada

Pieter R. Cullis – Department of Biochemistry and Molecular Biology, University of British Columbia, Vancouver, British Columbia V6T 1Z3, Canada; orcid.org/0000-0001-9586-2508

Complete contact information is available at:
<https://pubs.acs.org/10.1021/acsnano.2c10936>

Notes

The authors declare no competing financial interest.

ACKNOWLEDGMENTS

The authors would like to acknowledge Jennifer Lou for her help on plasmid amplification and James Jonkman at Advanced Optical Microscopy Facility (University Health Network, Toronto) for his suggestions on confocal imaging optimization. The authors also thank Dr. Ali Darbandi at SickKids Hospital (Toronto) for his help in preparing tissue grids for TEM. We also thank the UBC High Resolution Macromolecular Cryo-Electron Microscopy Facility (HRMEM) for their support with the cryo-EM imaging. This work was funded by the support of Princess Margaret Discovery to Impact Grant, New Frontiers in Research Fund (NFRFE-2020-00710), Terry Fox New Frontiers Program Project Grant (#1075, #1081), Nano-Medicines Innovation Network (NMIN), the Canadian Institutes of Health Research (FDN154326), the Centre for Pharmaceutical Oncology (CPO) Scholarship, the Canada Foundation for Innovation (NIF-21765) and the Canada Research Chairs Program (950-232468). M.H.Y.C is funded by NMIN postdoctoral fellowship in gene therapy.

REFERENCES

- (1) Damase, T. R.; Sukhovshin, R.; Boada, C.; Taraballi, F.; Pettigrew, R. I.; Cooke, J. P. The Limitless Future of RNA Therapeutics. *Front Bioeng Biotechnol* **2021**, *9*, 628137.
- (2) Wang, F.; Zuroske, T.; Watts, J. K. RNA Therapeutics on the Rise. *Nat. Rev. Drug Discovery* **2020**, *19* (7), 441–442.
- (3) Setten, R. L.; Rossi, J. J.; Han, S. The Current State and Future Directions of RNAi-Based Therapeutics. *Nat. Rev. Drug Discovery* **2019**, *18* (6), 421–446.
- (4) Kulkarni, J. A.; Witzigmann, D.; Chen, S.; Cullis, P. R.; van der Meel, R. Lipid Nanoparticle Technology for Clinical Translation of siRNA Therapeutics. *Acc. Chem. Res.* **2019**, *52* (9), 2435–2444.
- (5) Kulkarni, J. A.; Witzigmann, D.; Thomson, S. B.; Chen, S.; Leavitt, B. R.; Cullis, P. R.; van der Meel, R. The Current Landscape of Nucleic Acid Therapeutics. *Nat. Nanotechnol.* **2021**, *16* (6), 630–643.
- (6) Akinc, A.; Maier, M. A.; Manoharan, M.; Fitzgerald, K.; Jayaraman, M.; Barros, S.; Ansell, S.; Du, X.; Hope, M. J.; Madden, T. D.; Mui, B. L.; Semple, S. C.; Tam, Y. K.; Ciufolini, M.; Witzigmann, D.; Kulkarni, J. A.; van der Meel, R.; Cullis, P. R. The Onpatro Story and the Clinical Translation of Nanomedicines Containing Nucleic Acid-Based Drugs. *Nat. Nanotechnol.* **2019**, *14* (12), 1084–1087.
- (7) Gilleron, J.; Querbes, W.; Zeigerer, A.; Borodovsky, A.; Marsico, G.; Schubert, U.; Manygoats, K.; Seifert, S.; Andree, C.; Stöter, M.; Epstein-Barash, H.; Zhang, L.; Kotliansky, V.; Fitzgerald, K.; Fava, E.; Bickle, M.; Kalaidzidis, Y.; Akinc, A.; Maier, M.; Zerial, M. Image-Based

Analysis of Lipid Nanoparticle-Mediated siRNA Delivery, Intracellular Trafficking and Endosomal Escape. *Nat. Biotechnol.* **2013**, *31* (7), 638–646.

(8) Sahay, G.; Querbes, W.; Alabi, C.; Eltoukhy, A.; Sarkar, S.; Zurenko, C.; Karagiannis, E.; Love, K.; Chen, D.; Zoncu, R.; Buganim, Y.; Schroeder, A.; Langer, R.; Anderson, D. G. Efficiency of siRNA Delivery by Lipid Nanoparticles Is Limited by Endocytic Recycling. *Nat. Biotechnol.* **2013**, *31* (7), 653–658.

(9) Palankar, R.; Skirtach, A. G.; Kreft, O.; Bédard, M.; Garstka, M.; Gould, K.; Möhwald, H.; Sukhorukov, G. B.; Winterhalter, M.; Springer, S. Controlled Intracellular Release of Peptides from Microcapsules Enhances Antigen Presentation on MHC Class I Molecules. *Small* **2009**, *5* (19), 2168–2176.

(10) Carregal-Romero, S.; Ochs, M.; Rivera-Gil, P.; Ganas, C.; Pavlov, A. M.; Sukhorukov, G. B.; Parak, W. J. NIR-Light Triggered Delivery of Macromolecules into the Cytosol. *J. Controlled Release* **2012**, *159*, 120.

(11) Brkovic, N.; Zhang, L.; Peters, J. N.; Kleine-Doepke, S.; Parak, W. J.; Zhu, D. Quantitative Assessment of Endosomal Escape of Various Endocytosed Polymer-Encapsulated Molecular Cargos upon Photo-thermal Heating. *Small* **2020**, *16* (46), 2003639.

(12) Høget, A. Photochemical Internalisation in Drug and Gene Delivery. *Adv. Drug Delivery Rev.* **2004**, *56* (1), 95–115.

(13) Norum, O.-J.; Selbo, P. K.; Weyergang, A.; Giercksky, K.-E.; Berg, K. Photochemical Internalization (PCI) in Cancer Therapy: From Bench towards Bedside Medicine. *Journal of Photochemistry and Photobiology B: Biology* **2009**, *96* (2), 83–92.

(14) Jerjes, W.; Theodossiou, T. A.; Hirschberg, H.; Høget, A.; Weyergang, A.; Selbo, P. K.; Hamdoon, Z.; Hopper, C.; Berg, K. Photochemical Internalization for Intracellular Drug Delivery. From Basic Mechanisms to Clinical Research. *J. Clin. Med.* **2020**, *9* (2), 528.

(15) Dechene, A.; Kasper, S.; Olivecrona, H.; Schirra, J.; Trojan, J. Photochemical Internalization and Gemcitabine Combined with First-Line Chemotherapy in Perihilar Cholangiocarcinoma: Observations in Three Patients. *ENDOSCOPY INTERNATIONAL OPEN* **2020**, *08*, E1878–E1883.

(16) Otterhaug, T.; Janetzki, S.; Welters, M. J. P.; Hakerud, M.; Nedberg, A. G.; Edwards, V. T.; Boekstijn, S.; Loof, N. M.; Selbo, P. K.; Olivecrona, H.; van der Burg, S. H.; Høget, A. Photochemical Internalization Enhanced Vaccination Is Safe, and Gives Promising Cellular Immune Responses to an HPV Peptide-Based Vaccine in a Phase I Clinical Study in Healthy Volunteers. *Front. Immunol.* **2021**, *11*, 576756.

(17) Endoh, T.; Sisido, M.; Ohtsuki, T. Spatial Regulation of Specific Gene Expression through Photoactivation of RNAi. *J. Controlled Release* **2009**, *137* (3), 241–245.

(18) Ohtsuki, T.; Miki, S.; Kobayashi, S.; Haraguchi, T.; Nakata, E.; Hirakawa, K.; Sumita, K.; Watanabe, K.; Okazaki, S. The Molecular Mechanism of Photochemical Internalization of Cell Penetrating Peptide-Cargo-Photosensitizer Conjugates. *Sci. Rep.* **2016**, *5* (1), 18577.

(19) Shiraga, K.; Soe, T. H.; Matsumoto, S.; Watanabe, K.; Ohtsuki, T. Red and Near-Infrared Light-Directed Cytosolic Delivery of Two Different RNAs Using Photosensitive RNA Carriers. *Bioconjugate Chem.* **2018**, *29* (9), 3174–3179.

(20) Chen, W.; Deng, W.; Goldys, E. M. Light-Triggerable Liposomes for Enhanced Endolysosomal Escape and Gene Silencing in PC12 Cells. *Molecular Therapy - Nucleic Acids* **2017**, *7*, 366–377.

(21) Somiya, M.; Sakaeda, K.; Ishii, Y.; Kuroda, S. Cytoplasmic Delivery of Small Interfering RNA by Photoresponsive Non-Cationic Liposomes. *Journal of Drug Delivery Science and Technology* **2021**, *63*, 102488.

(22) Suzuki, I. L.; de Araujo, M. M.; Bagnato, V. S.; Bentley, M. V. L. B. TNF α siRNA Delivery by Nanoparticles and Photochemical Internalization for Psoriasis Topical Therapy. *J. Controlled Release* **2021**, *338*, 316–329.

(23) Soe, T. H.; Watanabe, K.; Ohtsuki, T. Photoinduced Endosomal Escape Mechanism: A View from Photochemical Internalization Mediated by CPP-Photosensitizer Conjugates. *Molecules* **2021**, *26* (1), 36.

(24) Saad, M. A.; Hasan, T. Spotlight on Photoactivatable Liposomes beyond Drug Delivery: An Enabler of Multitargeting of Molecular Pathways. *Bioconjugate Chem.* **2022**, *33* (11), 2041–2064.

(25) Lv, H.; Zhang, S.; Wang, B.; Cui, S.; Yan, J. Toxicity of Cationic Lipids and Cationic Polymers in Gene Delivery. *J. Controlled Release* **2006**, *114* (1), 100–109.

(26) Lovell, J. F.; Jin, C. S.; Huynh, E.; Jin, H.; Kim, C.; Rubinstein, J. L.; Chan, W. C. W.; Cao, W.; Wang, L. V.; Zheng, G. Porphosome Nanovesicles Generated by Porphyrin Bilayers for Use as Multimodal Biophotonic Contrast Agents. *Nature materials* **2011**, *10* (4), 324–332.

(27) Cui, L.; Lin, Q.; Jin, C. S.; Jiang, W.; Huang, H.; Ding, L.; Muhanna, N.; Irish, J. C.; Wang, F.; Chen, J.; Zheng, G. A PEGylation-Free Biomimetic Porphyrin Nanopatform for Personalized Cancer Theranostics. *ACS Nano* **2015**, *9* (4), 4484–4495.

(28) Huynh, E.; Leung, B. Y.; Helfield, B. L.; Shakiba, M.; Gandier, J. A.; Jin, C. S.; Master, E. R.; Wilson, B. C.; Goertz, D. E.; Zheng, G. In Situ Conversion of Porphyrin Microbubbles to Nanoparticles for Multimodality Imaging. *Nat. Nanotechnol* **2015**, *10* (4), 325–332.

(29) Chang, E.; Bu, J.; Ding, L.; Lou, J. W. H.; Valic, M. S.; Cheng, M. H. Y.; Rosilio, V.; Chen, J.; Zheng, G. Porphyrin-Lipid Stabilized Paclitaxel Nanoemulsion for Combined Photodynamic Therapy and Chemotherapy. *J. Nanobiotechnol.* **2021**, *19* (1), 154.

(30) Dolmans, D. E. J. G. J.; Fukumura, D.; Jain, R. K. Photodynamic Therapy for Cancer. *Nat. Rev. Cancer* **2003**, *3* (5), 380–387.

(31) Lovell, J. F.; Liu, T. W.; Chen, J.; Zheng, G. Activatable Photosensitizers for Imaging and Therapy. *Chem. Rev.* **2010**, *110* (5), 2839–2857.

(32) Rajora, M. A.; Lou, J. W. H.; Zheng, G. Advancing Porphyrin's Biomedical Utility via Supramolecular Chemistry. *Chem. Soc. Rev.* **2017**, *46* (21), 6433–6469.

(33) Belliveau, N. M.; Huft, J.; Lin, P. J.; Chen, S.; Leung, A. K.; Leaver, T. J.; Wild, A. W.; Lee, J. B.; Taylor, R. J.; Tam, Y. K.; Hansen, C. L.; Cullis, P. R. Microfluidic Synthesis of Highly Potent Limit-Size Lipid Nanoparticles for In Vivo Delivery of siRNA. *Molecular Therapy - Nucleic Acids* **2012**, *1*, e37.

(34) Scott, C. C.; Vacca, F.; Gruenberg, J. Endosome Maturation, Transport and Functions. *Seminars in Cell & Developmental Biology* **2014**, *31*, 2–10.

(35) Huotari, J.; Helenius, A. Endosome Maturation. *EMBO J.* **2011**, *30* (17), 3481–3500.

(36) Cullis, P. R.; Hope, M. J. Lipid Nanoparticle Systems for Enabling Gene Therapies. *Mol. Ther* **2017**, *25* (7), 1467–1475.

(37) Moan, J.; Berg, K. The Photodegradation of Porphyrins in Cells Can Be Used to Estimate the Lifetime of Singlet Oxygen. *Photochem. Photobiol.* **1991**, *53* (4), 549–553.

(38) Munson, M. J.; O'Driscoll, G.; Silva, A. M.; Lázaro-Ibáñez, E.; Gallud, A.; Wilson, J. T.; Collén, A.; Esbjörner, E. K.; Sabirsh, A. A High-Throughput Galectin-9 Imaging Assay for Quantifying Nanoparticle Uptake, Endosomal Escape and Functional RNA Delivery. *Commun. Biol.* **2021**, *4* (1), 211.

(39) Schroeder, A.; Levins, C. G.; Cortez, C.; Langer, R.; Anderson, D. G. Lipid-Based Nanotherapeutics for siRNA Delivery. *J. Intern Med.* **2010**, *267* (1), 9–21.

(40) Hedlund, H.; Rietz, H. D.; Johansson, J.; Zedan, W.; Huang, L.; Wallin, J.; Witttrup, A. Absolute Quantification and Single-Cell Dose-Response of Cytosolic siRNA Delivery. *bioRxiv*, April 22, 2021, ver. 1. DOI: 10.1101/2021.04.21.440807.

(41) Van de Vyver, T.; Bogaert, B.; De Backer, L.; Joris, F.; Guagliardo, R.; Van Hoeck, J.; Merckx, P.; Van Calenbergh, S.; Ramishetti, S.; Peer, D.; Remaut, K.; De Smedt, S. C.; Raemdonck, K. Cationic Amphiphilic Drugs Boost the Lysosomal Escape of Small Nucleic Acid Therapeutics in a Nanocarrier-Dependent Manner. *ACS Nano* **2020**, *14* (4), 4774–4791.

(42) Kulkarni, J. A.; Tam, Y. Y. C.; Chen, S.; Tam, Y. K.; Zaifman, J.; Cullis, P. R.; Biswas, S. Rapid Synthesis of Lipid Nanoparticles Containing Hydrophobic Inorganic Nanoparticles. *Nanoscale* **2017**, *9* (36), 13600–13609.

(43) Kulkarni, J. A.; Darjuan, M. M.; Mercer, J. E.; Chen, S.; van der Meel, R.; Thewalt, J. L.; Tam, Y. Y. C.; Cullis, P. R. On the Formation

and Morphology of Lipid Nanoparticles Containing Ionizable Cationic Lipids and siRNA. *ACS Nano* **2018**, *12* (5), 4787–4795.

(44) Dunn, K. W.; Kamocka, M. M.; McDonald, J. H. A Practical Guide to Evaluating Colocalization in Biological Microscopy. *American Journal of Physiology-Cell Physiology* **2011**, *300* (4), C723–C742.

(45) Al-Nasiry, S.; Geusens, N.; Hanssens, M.; Luyten, C.; Pijnenborg, R. The Use of Alamar Blue Assay for Quantitative Analysis of Viability, Migration and Invasion of Choriocarcinoma Cells. *Hum. Reprod.* **2007**, *22* (5), 1304–1309.

Recommended by ACS

Effective mRNA Delivery by Condensation with Cationic Nanogels Incorporated into Liposomes

Nevena Duskunovic, Hyun Jung Chung, *et al.*

MAY 15, 2023
MOLECULAR PHARMACEUTICS

READ 

Mechanistic Insights into the Superior DNA Delivery Efficiency of Multicomponent Lipid Nanoparticles: An In Vitro and In Vivo Study

Erica Quagliarini, Giulio Caracciolo, *et al.*

DECEMBER 16, 2022
ACS APPLIED MATERIALS & INTERFACES

READ 

Iterative Design of Ionizable Lipids for Intramuscular mRNA Delivery

Grayson Tilstra, Omar F. Khan, *et al.*

JANUARY 18, 2023
JOURNAL OF THE AMERICAN CHEMICAL SOCIETY

READ 

Leveraging Biological Buffers for Efficient Messenger RNA Delivery via Lipid Nanoparticles

Michael I. Henderson, Gaurav Sahay, *et al.*

SEPTEMBER 21, 2022
MOLECULAR PHARMACEUTICS

READ 

Get More Suggestions >